

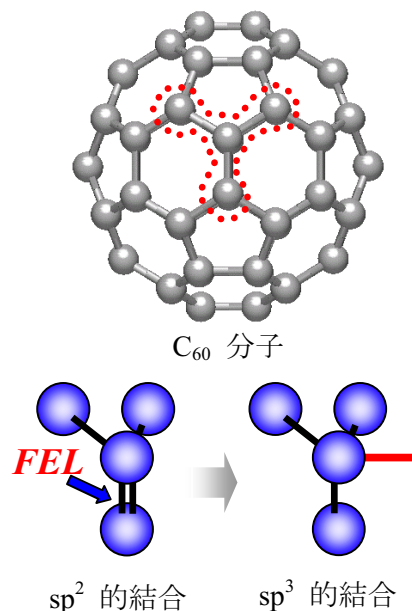
研究課題名：FEL による新素材の開発

研究代表者：山本 寛(日本大学理工学部電子情報工学科)

【研究目的】

本研究の目的は自由電子レーザー(FEL)を用いてマクロスケールの 3 次元 C₆₀ ポリマー (スーパーダイヤモンド) を合成するところにある。

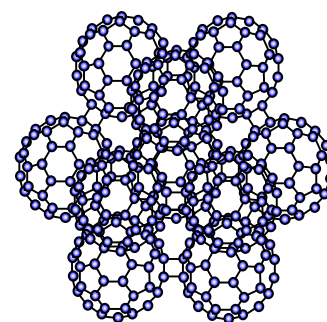
C₆₀ がポリマーを形成すると超硬質材料となる可能性があるため、高温高压プロセス研究がなされている。しかし、マクロスケールでの単相 3 次元ポリマー化は未だ確認されていない。そこで、本研究ではホールドーピングによる効果に注目した。ホールをドーピングすることで、C₆₀ の炭素原子のエネルギー状態は、超高压下 (数 GPa) における状況と同一視することができる^[1]。アクセプタ元素と C₆₀ 混合物にレーザー照射することで、電子励起・移動させ、ポリマー化反応の促進を計った。光源には、可変波長特性と大出力を有する FEL を採用した。



【研究概要】

スーパーダイヤモンド

図 1 にスーパーダイヤモンドの合成原理を示す。1 つの炭素原子は二重結合を含む sp² 的な結合で存在している。その二重結合を光エネルギーで打ち切り、余った電子を隣接する C₆₀ 分子との共有結合に使う。これを連続かつ 3 次的に進めることでスーパーダイヤモンドは合成される。それは C₆₀ の性質上、超硬質・超軽量・超柔軟という 3 つの驚異的特徴を示すものと考えている。元々硬い C₆₀ がダイヤモンドに代表される sp³ 的結合で稠密構造をとると、ダイヤモンド級の硬度に加えて、内部空洞により低密度かつ軽量となる。また、C₆₀ 分子が接点でのみ結合した非晶質構造は、弾性・粘性に富むと考える。これらの性質から、スーパーダイヤモンドはマイクロ・ナノデバイス、航空宇宙や建築、自動車の新しい構造材料、医療インプラントなど、様々な分野で活躍できる新素材となるものと期待される。



スーパーダイヤモンド

図 1. スーパーダイヤモンド合成原理と分子集合イメージ図

実験

試料は真空中で加圧・紫外線照射することにより作製した。C₆₀ 粉末のみのサンプルと、アクセプタとして I₂ を重量比 1:1 で混入した 2 パターンを使用し、I₂ の有無による違い

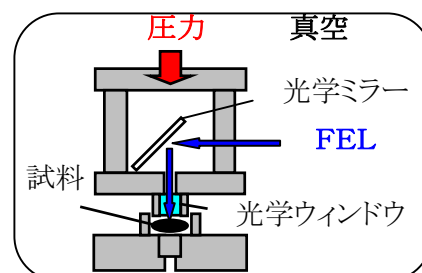


図 2. 実験装置図

でホールドープの効果を評価した。レーザ波長は基本波 1450nm と 3 倍高調波の 450nm を照射した。これはベンゼン環の結合エネルギーより見積った、 C_{60} の二重結合を打ち切るのに必要なエネルギーをもった波長である。レーザ強度は 数 $10\mu\text{J}/\text{Pulse}$ 、繰り返し照射周波数 2Hz で 300min 照射した。評価装置にはラマン分光、XRD を使用した。

結果・考察

図 3 に XRD パターンを示す。FEL 照射により各々の面において回折角の増加、 I_2 混合サンプルでは (111)、(222) 面をはじめ、各ピーク強度の著しい減少とピーク強度比の変化を確認した。また、 $C_{60}(I_2)_x$ と見られるピーク (図中矢印) も現れた。

回折角の増加は面間隔の縮小を意味し、ピーク強度の変化は結晶性の低下を示す。サンプルが完全に層間化合物 $C_{60}(I_2)_x$ を形成している場合、本来 C_{60} のもっている (111) 面のピークは消失するはずであり、結果グラフとは一致しない。このことから、 I_2 はホールドナーとして振舞う一方、一部で C_{60} と層間化合物を形成したと考えられる。

図 4 にラマン分光の測定結果を示す。FEL 照射により $Ag(2)$ 振動モードの波数が 3.2cm^{-1} マイナス側にシフトし、 I_2 混入サンプルにおいては 7.5cm^{-1} の大きなシフトを確認した。

$Ag(2)$ モードとは、グラフに示すように、各炭素原子が五員環の中心に集まるように振動するモードである。 C_{60} がポリマー化すると分子間に発生する結合によって C_{60} を構成する炭素原子間の距離が若干変化し、それに伴い振動が制限され、結果として振動数の変化につながる。二量体 (ダイマー) を形成するところの $Ag(2)$ モードが 10cm^{-1} マイナス側へシフトするとの報告^[2]があるが、 C_{60} が 3 次元的にポリマー化した場合どの程度シフトするのか明確な値は明らかになっていない。ただ、ダイマー化より複雑に結合する 3 次元ポリマー化は、その振動制限も激しく、シフトも大きいと予想される。このことから、 I_2 を混入しホールドープしたことで、より大きなシフトを確認したことは、ホールドープがポリマー化に有効であることを示唆している^[3]。

【まとめ】

XRD より、結晶性の低下、一部で層間化合物 $C_{60}(I_2)_x$ の形成を確認した。ラマン分光により、 $Ag(2)$ モードが 7.5cm^{-1} シフトすることを確認し、ホールドープがポリマー化を促進したことを確認した。今回、所望するスーパーダイヤモンドを得るには至らなかったが、光励起ホールドープと

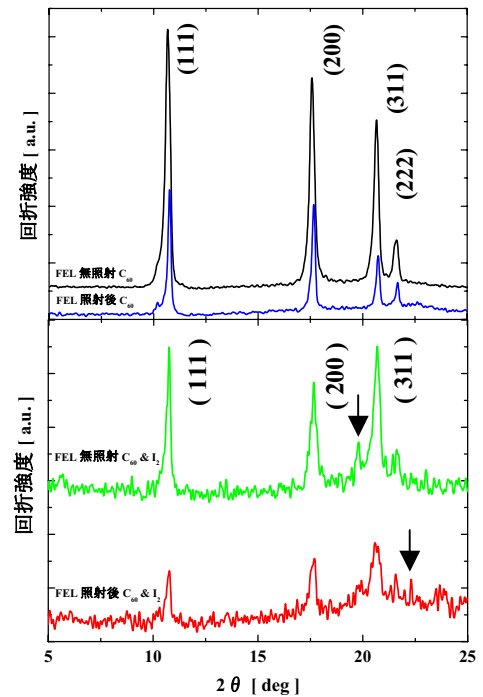


図 3. XRD パターン

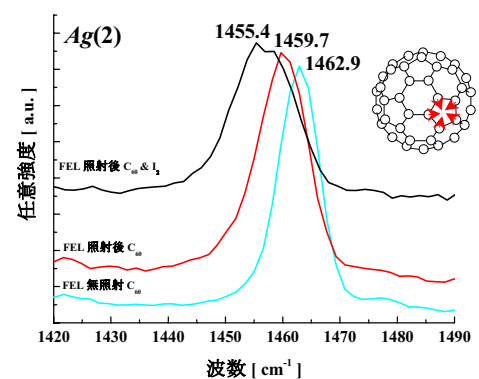


図 4. ラマン分光

いうアプローチで C_{60} の物性が変化することを確認した。これはスーパーダイヤモンドが合成可能であることを示唆しており、今後形成条件の最適化をはかることによって、夢の新素材を創製することが出来るものと期待される。

参考文献

- [1] Hiroyuki Nakayama and Hiroshi Katayama, *Jan.J.Appl.Phys*, **41**(2002)817.
- [2] G. B. Adams et al., *Phys. Rev. B*, **50**(1994)15.
- [3] 橋本, 石川, 岩田, 山本, 第 52 回応用物理学関係連合講演会, 31p-ZC-9(2005).

【研究業績等】

・ 発表論文

- (1) Y. Shimizu, K. Saito, T. Sakuma, N. Iwata and H. Yamamoto: “Electronic Transportation Anomaly Observed in Interfaces of Nanostructured C₆₀ Monolayers and Ultrathin Au Films”, Proceeding of IUMRS-ICA 2004(Tsintsu, Taiwan, 17-18th Nov. 2004),(2005)pp.1-6.
- (2) N. Iwata, K. Fukai and H. Yamamoto: “Crystallization and Conductivity of ReO₃ Thin Films Prepared by 90° Off-Axis RF Magnetron Sputtering Method”, IEICE Trans. Electron, **E87-C** (2004) pp.223-226
- (3) Y. Shimizu, K. Saito, T. Sakuma, N. Iwata and H. Yamamoto: “Electronic Transport Properties of C₆₀ Derivative Self-Assembly Monolayer on Au Ultrathin Film”, Trans. of the Mate. Res. Soc. Jpn., **29** (2004) 1323-1326.
- (4) T. Kato, S. Yamaguchi, A. Takahashi, N. Iwata and H. Yamamoto: “Chromogenic Responses Induced by Electric Field in Phthalocyanine Derivative LB Films”, Trans. of the Mate. Res. Soc. Jpn., **29** (2004) 759-762.
- (5) A. Noguchi, J. Kurian, T. Amemura, K. Tanabe, T. Morishita, N. Iwata, H. Yamamoto, M.Kusunoki, M. Mukaida and S. Ohshima: “Preparation and Characterization of NdBa₂Cu₃O_{7-δ} thin films on MgO substrates with Ba₂NdTaO₆ buffer layers”, Trans. of the Mate. Res. Soc. Jpn., **29** (2004) 1269-1272.
- (6) K. Fukai, M. Masui, N. Iwata and H. Yamamoto: “Conductive Properties of ReO₃ / SrCuO₂ Bilayered Films”, Trans. of the Mate. Res. Soc. Jpn., **29** (2004) 1315-1318.
- (7) Y. Nakajima, H. Kokubun, T. Amemura, N. Iwata, Y. Tarutani, K. Tanabe, T. Morishita and H. Yamamoto: “Preparation of Josephson Junctions by MOCVD films”, Trans. of the Mate. Res. Soc. Jpn., **29** (2004) 1331-1334.
- (8) N. Iwata, K. Matsuo and H. Yamamoto: “Preparations and Evaluations of Magnetoelectric Oxides / Superconductor Multilayers”, Trans. of the Mate. Res. Soc. Jpn., **29** (2004) 1437-1440.
- (9) H. Yamamoto, N. Iwata, and Y. Shimizu: “Nano-Structured C₆₀-SAM Formed on Ultrathin Au Films/MgO Single Crystal”, Technical Proceedings of NSTI Nanotech **3** (2004) pp. 441-444.
- (10) N. Iwata, K. Matsuo, N. Ootsuka and H. Yamamoto: “Preparations and Evaluations of Magnetoelectric Thin Films for Josephson Field Effect Transistor”, Mat. Res. Soc. Symp. Proc., **811** (2004) pp.425-430.
- (11) 中嶋, 国分, 飴村, 岩田, 樽谷, 田辺, 森下, 山本, 全工程 MOCVD 法によるジョセフソン接合の作製, 電子情報通信学会技術報告, SCE2003-2(April 2003) pp.9-13.
- (12) 奥山, 金城, 岩田, 山本, C₆₀ 低次元ナノ構造超薄膜の形成, 電子情報通信学会技術報告, Vol.103, No.245(2003)pp.1-6.
- (13) 奥山, 金城, 長山, 岩田, 山本, 再蒸発法による C₆₀ 超薄膜ナノ構造, 電子情報通信学会技術研究報告, Vol. 103, No.411(2003)pp.27-32.
- (14) 深井, 榊井, 岩田, 山本, スパッタ法による ReO₃/SrCuO₂ 積層膜の作製, 電子情報通信学会技術研究報告, Vol. 103, No.411(2003)pp.33-38.
- (15) H. Yamamoto, K. Fukai, K. Matsuo, N. Iwata, Optical and conductive properties of ReO₃ sputtered thin films, Proc. of The 7th International Symposium on Sputtering & Plasma Processes-ISSP2003-(2003) pp.206-209.
- (16) Nobuyuki Iwata, Keigo Mukaimoto, Hiroyuki Imai and Hiroshi Yamamoto, Transport properties of C₆₀ ultra-thin films, Surf. Coat. Tech. **169-170** (2003)pp. 646-649.

- (17) N. Iwata and H. Yamamoto, SYNTHESIS OF SINGLE-CRYSTALLINE C₆₀ ULTRATHIN FILMS BY VACUUM EVAPORATION, Proceeding of “1st International Conference on Materials Processing for Properties and Performance[MP3]”, Eds by K. H. Khor, S. Y. Zhang, P. Hing, and F. Boey, Institute of Materials [East Asia], (2003) pp.772-779.
- (18) N. Iwata and H. Yamamoto, Synthesis of C₆₀ Monolayer with One-Dimensional Nano-Structure, Proc. of The 5th Joint Seminar of China-Japanese Amity Universities, pp.54-59(2003).
- (19) K. Onozuka, N. Iwata, and H. Yamamoto: Novel vacuum system for in-situ characterization of fluorescence properties of thin films, Int. J. Mod. Phys. B, 16, 28&29(2002)pp.4445-4448.
- (20) K. Suzuki, M. Okamoto, S. Alsadoon, N. Iwata, H. Yamamoto: Chromogenic properties of Phthalocyanine Derivatives Langmuir-Blodgett Films, Trans. Mate. Res. Soc. Jpn., Vol. 27, No. 2(2002)pp345-348.
- (21) M. Ohkubo, K. Fukai, N. Iwata and H. Yamamoto: Preparations of conductive ReO₃ thin films, Superconductor Science and Technology (SuST), Vol. 15, No. 12(2002)pp.1778-1780.
- (22) H. Imai, N. Iwata and H. Yamamoto: Synthesis of C₆₀ self-assembled monolayer on Au ultrathin films, Nanotechnology, Vol. 13(2002)pp.768-770.
- (23) M. Ohkubo, K. Fukai, N. Iwata, and H. Yamamoto: Preparation of Conductive Re Oxide Thin Films by Sputtering, Technical Report of IEICE, Vol.102, No.434(2002)pp.23-28. (in Japanese)
- (24) N. Iwata, H. Okuyama, S. Kuroda, Y. Shimizu, H. Imai, and H. Yamamoto: Low Dimensional Nano-Structure of C₆₀ Thin Films, Technical Report of IEICE, Vol.102, No.260(2002)pp.13-17. (in Japanese)
- (25) H. Yamamoto, H. Isogai, and Y. Yoshida: Low-voltage electron beam excitement luminescence of oxide thin films with multilayered structure, Thin Solid Films,383(2001)pp.89-91.
- (26) N. Iwata, N. Hashimoto, and H. Yamamoto: Preparation of Continuous C₆₀ Thin Films with Flat Surfaces by Vacuum Evaporation, Trans. of the MRS-J, Vol. 26, No. 4(2001)pp.1339-1342.
- (27) K. Suzuki, T. Kato, Y. Nakamura, N. Iwata, and H. Yamamoto: Preparation of Phthalocyanine Derivative Ultrathin Films by Langmuir-Blodgett Method, Trans. of the MRS-J, Vol. 26, No. 4(2001)pp.1335-1338.
- (28) 岩田展幸、向本圭吾、清水利枝、今井博行、山本寛: 「C₆₀ 薄膜の電界効果をめざして」, 電子情報通信学会技術研究報告, CPM2001-103, Vol.101 (2001-10)pp.67-72.
- (29) 今井博行、小林寛、清水利枝、岩田展幸、山本寛, 「C₆₀ 誘導体自己組織単分子膜の作製と評価」, 電子情報通信学会技術研究報告書, CPM2001-104, Vol. 101(2001-10) pp.73-78.
- (30) 大久保学、松尾幸治、岩田展幸、山本寛, 「Re 酸化物薄膜の発色と伝導性」, 電子情報通信学会技術研究報告, CPM2001-110, Vol.101(2001-10) pp.107-112.
- (31) N. Iwata, Y. Ishii, H. Yamamoto, H. Zama, T. Morishita, and K. Kohn: Ferromagnetic Insulator EuO Thin Film, Ferrites : Proceedings of ICF8, (2000)pp.642-644.

• 学会発表

8th International Superconductive Electronics Conference ISEC'01, Osaka Sun Palace, Osaka, Japan, 2001.06.19-06.22

- (1) Nobuyuki Iwata, Hiroyuki Imai, Hiroshi Yamamoto, Experimental Verification of Superconductivity

Expected in Interface of Dielectric and C60 Thin films, P1-G8

International Conference on Materials for Advanced Technologies (ICMAT'01), Singapore

International Convention & Exhibition Centre, 2001.07.01-07.06

- (1) Nobuyuki Iwata, Manabu Ohkubo and Hiroshi Yamamoto, Preparations of ReOx thin films and SrCuO2 / ReOx multilayered films, P12-11

VII International Conference on Advanced Materials (ICAM 2001) , J.W.Marriott, Punta Cancun, Cancun Quintana-Roo, Mexico, 2001.08.26-08.30

- (1) (Invited) Hiroshi Yamamoto, Nobuyuki Iwata, Hiroyuki Imai and Keigo Mukaimoto, Synthesis and properties of very smooth C60 ultrathin films by vacuum evaporation, 13-7SA

Frontiers of Surface Engineering 2001 (FSE2001) Conference and Exhibition, Nagoya Congress Center, Nagoya, Japan, 2001.10.28-11.01

- (1) Nobuyuki Iwata, Keigo Mukaimoto, Hiroyuki Imai and Hiroshi Yamamoto, Transport Properties of C60 ultrathin films, D4-14

First East Asia Symposium on Superconductive Electronics EASSE 2001, New Industry Creation Hatchery Center (NICHe), Tohoku University, Sendai, 2001.11.26-11.28

- (1) Estimation of Cooling Performance of Pulse Tube Cryocooler, PS-23

XUT-NU JOINT SYMPOSIUM ON ELECTRICAL ENGINEERING AND ELECTRONIC AND COMPUTER SCIENCE, Xi'an University of Technology, 2001.9.21

- (1) Hiroahi Yamamoto and Nobuyuki Iwata, NANO-SYNTHESIS PROCESS AIMING AT MOLECULAR ELECTRONICS

第 8 回電気学会 有機薄膜・分子超薄膜及び有機・無機複合膜の機能化調査専門委員会, 東京工業大学, 2001.10.28

- (1) 山本寛、岩田展幸, NANO-SYNTHESIS PROCESS AIMING AT MOLECULAR ELECTRONICS

電子情報通信学会 電子部品材料研究会-薄膜プロセス・材料, 信州大学工学部, 2001.10.26

- (1) 今井博行、小林寛、清水利枝、岩田展幸、山本寛, C60 誘導体自己組織単分子膜の作製と評価, CPM2001-104

- (2) 大久保学、松尾幸治、岩田展幸、山本寛, Re 酸化物薄膜の発色と伝導性, CPM2001-110

- (3) 岩田展幸、向本圭吾、清水利枝、今井博行、山本寛, C60 薄膜の電界効果をめざして, CPM2001-103

学会名: 電子情報通信学会研究会 (電子部品・材料) -薄膜プロセス・材料、一般-

第 45 回理工学部学術講演会 (材料・物性部会, 日本大学理工学部船橋校舎 (13 号館) , 2001.11.13

- (1) 小林寛、今井博行、清水利枝、岩田展幸、山本寛, C60 誘導体による自己組織単分子膜の作製, Ca6

- (2) 中嶋雄一、岩田展幸、山本寛、高橋義広、森下忠隆, MOCVD 法による Sr2AlTaO6 絶縁薄膜の基板温度特性, Ca4

- (3) 松尾幸治、大久保学、岩田展幸、山本寛, 反応性 RF スパッタによる Re 酸化物薄膜の作製と評価, Ca3

- (4) 岡本 正史、鈴木 航也、Alsadoon Saliman、岩田 展幸、山本 寛, フタロシアニン誘導体 LB 薄膜の構造評価とクロミズム, Ca7

- (5) 李 度協、小野塚 浩平、岩田 展幸、山本 寛, 有機 EL 用蛍光薄膜の作製と評価, Ca8

- (6) 櫻沢 真人、岩田 展幸、山本 寛、戴 巍、松原 洋一, パルス管冷凍機の冷凍特性予測, Cp9

- (7) 向本圭吾、岩田展幸、山本寛, C60 薄膜の作製と結晶評価, Ca5

(8) 野口章、岩田展幸、山本寛、森下忠隆, オフアクシス DC-RF ハイブリッドマグネトロンプラズマスパッタリング法による NdBa₂Cu₃O_{7-d} 薄膜の作製と評価, Ca2

電気化学会第 68 回大会, 神戸大学工学部, 2001.4.1-3

- (1) 大久保学, 武井辰憲, 岩田展幸, 山本寛, Re 酸化物膜の光吸収スペクトル, 1I32
- (2) 鈴木 航也、加藤敬幸、中村 雄一、岩田 展幸、山本 寛, フタロシアニン誘導体 LB 超薄膜作製とクロミズム, 1 I 31

平成 13 年度日本写真学会, 千葉大学けやき会館, 2001.5.22-23

(1) 鈴木 航也、加藤敬幸、岩田 展幸、山本 寛, LB 法によるフタロシアニン誘導体膜の作製, C05
第 13 回 日本 MRS 学術シンポジウム, 神奈川県サイエンスパーク, 2001.12.21

- (1) 清水利枝、小林寛、今井博行、岩田展幸、山本寛, Preparations and Evaluations of Self - Assembly Monolayers of C60 Derivatives, B2-P10-M
- (2) 鈴木 航也、岡本 正史、Alsadoon Saliman、岩田 展幸、山本 寛, フタロシアニン誘導体 LB 膜のクロモジェニック特性, G01-O03

第 49 回応用物理学関係連合講演会, 東海大学、湘南校舎, 2002.3.27-30

- (1) 今井博行、小林寛、清水利枝、岩田展幸、山本寛, C60 誘導体自己組織単分子膜の作製と電気伝導特性, 29p-YN-12
- (2) 海老沢憲一、陳健、中島健介、山下努、櫻沢真人、山本寛、松原洋一, 小型パルス管冷凍機に搭載した高温超伝導ジョセフソン接合のノイズ特性, 29a-ZS-10

第 66 回 2002 年度春季 低温工学・超伝導学会, 工学院大学 新宿校舎, 2002.5.18-20

- (1) 櫻沢真人 岩田展幸 山本寛 戴巍 松原洋一, J J 素子冷却のためのパルス管冷凍機, D3-2

The 8th International Union of Materials Research Societies (IUMRS) - International Conference on Electronic Materials (ICEM), 西安、曲江賓館, 2002.6.10-14

- (1) Hiroyuki Imai, Nobuyuki Iwata and Hiroshi Yamamoto, Synthesis of C60-SAM on Au ultrathin films, E40
- (2) Manabu Ohkubo, Kumiko Fukai, Nobuyuki Iwata and Hiroshi Yamamoto, Preparations of conductive ReO₃ thin films, L86
- (3) Nobuyuki Iwata, Shinji Kuroda, Hiroki Okuyama and Hiroshi Yamamoto, Transport properties of C60 thin films, E41
- (4) Takayuki Kato, Saliman Alsadoon, Nobuyuki Iwata and Hiroshi Yamamoto, Electrochromic properties of Phthalocyanine derivative Langmuir -Blodgett films, E39
- (5) Kohei Onozuka, Nobuyuki Iwata, and Hiroshi Yamamoto, Novel vacuum system for in-situ characterization of fluorescence properties of thin films, H63

第 23 回フラーレン・ナノチューブ総合シンポジウム, 松島、ホテル松島大観荘, 2002.7.17-19

- (1) Nobuyuki Iwata, Hiroki Okuyama, Shinji Kuroda, Hiroyuki Imai, Yoshiki Shimizu, and Hiroshi Yamamoto, Low Dimensional Nano-Structure for C60, 1P-51

電子情報通信学会電子部品・材料研究会, 盛岡、岩手大学, 2002.8.8

- (1) 岩田展幸、奥山博基、黒田真司、清水芳貴、今井博行、山本寛, C60 薄膜の低次元ナノ構造, CPM2002-53

The 2nd International Meeting on Information Display, 韓国、大邱 EXCO, 2002.8.21-23

- (1) (Invited)Takayuki Kato, Saliman Alsadoon, Nobuyuki Iwata and Hiroshi Yamamoto, Novel Chromogenic

Materials Expected for Future FPD, 16.2

1st International Conference on Materials Processing for Properties and Performance (MP3), シンガポール、コンラッド・センテナリアル・シンガポール, 2002.8.1-3

(1) Nobuyuki Iwata and Hiroshi Yamamoto, SYNTHESIS OF SINGLE-CRYSTALLINE C60 ULTRATHIN FILMS BY VACUUM EVAPORATION, Thin Films & Coatings Session #2-3

The 4th Joint Seminar of NU-XUT, 日本大学理工学部、船橋校舎, 2002.9.9

(1) Nobuyuki IWATA and Hiroshi YAMAMOTO, Materials Science of C60 Ultrathin Films

第 63 回応用物理学会学術講演会, 新潟、新潟大学, 2002.9.24-27

(1) 野口章、J.Kurian、飴村隆、岩田展幸、田辺圭一、森下忠隆、山本寛, $T_c > 91\text{K}$, $\text{NdBa}_2\text{Cu}_3\text{O}_{7-\delta}$ 薄膜のための $\text{Ba}_2\text{NdTaO}_6$ バッファ付き MgO 基板, 26p-H-12/I

(2) 中嶋雄一、岩田展幸、田辺圭一、森下忠隆、山本寛, $\text{YBa}_2\text{Cu}_3\text{O}_{7-x}$ 厚膜上に積層した $\text{Sr}_2\text{AlTaO}_6$ 薄膜表面にあらわれる粒子の発生原因, 26a-H-8/I

第 67 回 2002 年度秋季 低温工学・超伝導学会, 長崎ブリックホール, 2002.10.30-11.1

(1) 海老沢憲一、陳健、中島健介、山下努、櫻沢真人、山本寛、松原洋一, 小型パルス管冷凍機に搭載した高温超伝導ジョセフソン接合のノイズ特性, 3D-a08

第 45 回理工学部学術講演会, 日本大学理工学部、船橋校舎, 2002.11.20

(1) 山口壮樹、加藤敬幸、Alsadoon Saliman、岩田展幸、山本寛, ITO 基板表面状態の違いによる LB 薄膜の構造・光吸収特性

(2) 米増拓郎、小野塚浩平、岩田展幸、山本 寛, 有機材料の蛍光発光機構の検討

(3) 奥山博基、岩田展幸、山本寛, C60 超薄膜の低次元ナノ構造

(4) 黒田真司、岩田展幸、山本寛, 電界効果トランジスターを目指した C60 超薄膜の作製と電気伝導性

(5) 西村保広、今井博行、清水芳貴、岩田展幸、山本寛, C60 誘導体自己組織単分子膜の作製とその電気伝導特性

(6) 石川貴之、今井博行、岩田展幸、山本寛, C60 ポリマー化反応によるスーパーダイヤモンド合成

(7) 櫻沢真人 小林啓志 山本寛 松原洋一 都丸隆行, インライン型パルス管冷凍機の振動測定

電子情報通信学会電子部品・材料研究会, 新潟、新潟大学, 2002.11.13

(1) 大久保学、深井久美子、岩田展幸、山本寛, スパッタによる導電性 Re 酸化物薄膜の作製, CPM2002-116

Materials Research Society Fall Meeting, ボストン、ハイネス・コンベンション・センター, 2002.12.2-6

(1) Nobuyuki Iwata, Shinji Kuroda, Hiroki Okuyama, Hiroshi Yamamoto, SYNHESES OF C60 THIN FILMS WITH THICKNESS OF NANO-SCALE, I3.30

(2) Manabu Ohkubo, Kumiko Fukai, Kohji Matsuo, Nobuyuki Iwata, Hiroshi Yamamoto, INTERFACE CONDUCTION BETWEEN CONDUCTIVE ReO_3 THIN FILM AND $\text{NdBa}_2\text{Cu}_3\text{O}_6$, Z5.7

第 14 回日本 MRS 学術シンポジウム, 東京、東京工業大学 (大岡山), 2002.12.20-21

(1) Takayuki Kato, Souki Yamaguchi, Saliman Alsadoon, Nobuyuki Iwata and Hiroshi Yamamoto, PHTHALOCYANINE DERIVATIVES LB FILMS ACCUMULATED ON ITO GLASSES, E2-P11-M

(2) Kumiko Fukai, Manabu Ohkubo, Nobuyuki Iwata and Hiroshi Yamamoto, PREPARATION OF CONDUCTIVE ReO_3 THIN FILMS BY RF SPUTTERING, M2-P08-M

(3) Hiroyuki Imai, Yasuhiro Nishimura, Nobuyuki Iwata and Hiroshi Yamamoto, SYNTHESIS OF C60-SAM ON Au ULTRATHIN FILMS, A1-P24-M

H15 年電気学会全国大会, 東北学院大学, 2003.03.19

(1) 山本, 岩田, 有機薄膜及び有機・無機複合膜の新機能発現とデバイス応用, シンポジウム 2S7-8
第 50 回応用物理学関係連合講演会, 神奈川大学横浜キャンパス, 2003.3.27-30

(1) 奥山, 岩田, 山本, C₆₀ 超薄膜の低次元ナノ構造, 28p-B-11

(2) 海老沢, 陳, 中島, 山下, 櫻沢, 山本, 松原, 小型パルス管冷凍機に搭載した高温超伝導ジョセフソン接合のノイズ特性, 29a-ZS-10

(3) 今井, 小林, 清水, 岩田, 山本, C60誘導体自己組織単分子膜の作製と電気伝導特性, 29p-YN-12

(4) 深井, 大久保, 岩田, 山本, ReO₃ 薄膜の電気伝導性, 27p-S-16

(5) 加藤, 山口, Saliman Alsadoon, 岩田, 山本, 基板平滑性の違いによるアラキジン酸/フタロシアニン誘導体混合 LB 膜の配向度変化, 28p-C-1

電子情報通信学会 SCE 研究会, 機械振興会館, 東京, 2003.04.

(1) 中嶋, 国分, 飴村, 岩田, 樽谷, 田辺, 森下, 山本, 全工程 MOCVD 法によるジョセフソン接合の作製, SCE2003-2

第68回2003年度春季 低温工学・超伝導学会, 産業技術研究所つくばセンター 共同講堂, 2003.05.21,22,23

(1) 櫻沢, 小林, 山本, 八十濱, 松原, 秋田, 笠原, パルス管冷凍機用イナータンチューブの周波数特性, 2C-a10

The 7th International Symposium on Sputtering & Plasma Processes, Kokusai Hotel, Kanazawa, 2003.06.11-13

(1) H. Yamamoto, K. Fukai, K. Matsuo, N. Iwata, Optical and conductive properties of ReO₃ sputtered thin films, TF 3-5

第 25 回フラーレン・ナノチューブ総合シンポジウム, 淡路夢舞台国際会議場, 2003.07.23-25

(1) Nobuyuki Iwata, Hiroki Okuyama, Akane Kinjo and Hiroshi Yamamoto, Low Dimensional Alignment of C60 Molecules Prepared on Thermal Treated Substrates, 1P-57

電子情報通信学会 CPM 研究会, 網走グランドホテル, 2003.08.01

(1) 奥山, 金城, 岩田, 山本, C₆₀ 低次元ナノ構造超薄膜の形成, CPM2003-61

第64回応用物理学学会学術講演会, 福岡大学七隈キャンパス, 2003.08.30- 09. 2

(1) 海老沢, 陳, 中島, 山下, 櫻沢, 山本, 松原, 小型パルス管冷凍機を用いた高温超伝導ジョセフソン高周波検出システム, 31a-ZS-10

(2) 中嶋, 国分, 飴村, 岩田, 樽谷, 田辺, 森下, 山本, MOCVD法によるNdBa₂Cu₃O_{7-x}ランプエッジ接合の作製, 2a-N-9

(3) 野口, J. Kurian, 飴村, 岩田, 楠, 田辺, 森下, 山本, Ba₂NdTaO₆ バッファ層を用いた MgO 基板上の NdBa₂Cu₃O_{7-d} 薄膜の作製と評価, 30a-K-11

(4) 清水, 齊藤, 佐久間, 岩田, 山本, C₆₀ 誘導体自己組織単分子膜の電気伝導特性, 2a-L-5

(5) 松尾, 岩田, 山本, 電気磁気効果薄膜作製とその応用, 30p-T-13

(6) 奥山, 金城, 岩田, 山本, 基板ステップ拡散障壁を利用した C₆₀/金属の低次元ナノ構造, 30a-YL-8

(7) 梶井, 深井, 岩田, 山本, ReO₃ 薄膜の結晶性と電気伝導性, 30p-ZA-2

- (8) 山口, 加藤, 高橋, 岩田, 山本, アラキジン酸/フタロシアニン誘導体混合 LB 膜の表面観察, 2a-L-6

The 5th Joint Seminar of China-Japanese Amity Universities, X'ian University of Technology, X'ian, China, 2003.09.09

- (1) N. Iwata and H. Yamamoto, Synthesis of C₆₀ Monolayer with One-Dimensional Nano-Structure

The 8th IUMRS International Conference on Advanced Materials (IUMRS-ICAM 2003), Pacifico Yokohama, Conference Center, Yokohama, Japan, 2003.10.08-13

- (1) N. Iwata, H. Okuyama, A. Kinjo and H Yamamoto, One Dimensional Alignment of C₆₀ Molecules Prepared on Thermal Treated Substrates, A4-09-O07
- (2) T. Kato, S. Yamaguchi, A. Takahashi, N. Iwata, H. Yamamoto, Chromogenic Responses Induced by Electric Field in Phthalocyanine Derivative LB Films, B2-11-O05
- (3) A. Noguchi, J. Kurian, T. Amemura, K. Tanabe, T. Morishita, N. Iwata, H. Yamamoto, M. Kusunoki, M. Mukaïda, S. Ohshima, Preparation and Characterization of NdBa₂Cu₃O_{7-x} / Ba₂Nd TaO₆ // MgO multilayer films, B7-12-O07
- (4) K. Fukai, M. Masui, N. Iwata and H. Yamamoto, Conductive Properties of ReO₃/SrCuO₂ Bilayered Films, B7-13-O04
- (5) Y. Shimizu, K. Saito, T. Sakuma, N. Iwata and H. Yamamoto, Electronic Transport Properties of C₆₀ Derivative Self-Assembly Monolayer on Au Ultrathin Film, B7-13-O07
- (6) Y. Nakajima, H. Kokubun, T. Amemura, N. Iwata, Y. Tarutani, K. Tanabe, T. Morishita and H. Yamamoto, Preparation of Josephson Junctions by MOCVD films, B7-13-O10
- (7) N. Iwata, K. Matsuo and H Yamamoto, Preparations and Evaluations of Magneto-Electric Oxides / Superconductor Multilayers, B8-13-O15

第 47 回理工学部学術講演会, 日本大学理工学部船橋校舎, 2003.11.19

- (1) 長山, 奥山, 岩田, 山本, 有機 FET を目指した C₆₀/CaF₂//Si(111)の積層膜成長, 材料・物性部会 Cp38.
- (2) 金城, 奥山, 岩田, 山本, 基板ステップを利用した Au 粒子の低次元ナノ構造, 材料・物性部会 Cp36.
- (3) 橋本, 石川, 岩田, 山本, 高圧下・光励起による C₆₀ ポリマーの合成 Cp37.
- (4) 森本, 岩田, 樽谷, 田辺, 山本, SFQ-dc 変換回路をはじめとする SFQ 要素回路の設計とシミュレーション, Cp41
- (5) 樋口, 中嶋, 若菜, 岩田, 安達, 田辺, 山本, 超伝導薄膜の膜質がジョセフソン接合特性に与える影響, Cp40
- (6) 梶井, 深井, 岩田, 山本, ReO₃ 薄膜の結晶性と電気伝導性に与えるアニールの影響, Cp39
- (7) 高橋, 加藤, 山口, 岩田, 山本, アラキジン酸/フタロシアニン誘導体混合 LB 膜の高配向化と光吸収, Cp35

第 69 回 2003 年度秋季 低温工学・超伝導学会, 島根県民会館, 2003.12.3,4,5

- (1) 黒田, 櫻沢, 八十濱, 松原, 山本, 多層蓄冷器を用いた小型パルス管冷凍機の特長, 2C-a03
- (2) 櫻沢, 黒田, 小林, 山本, 八十濱, 松原, 秋田, 笠原, スターリング型パルス管冷凍機の試作, 2C-a02
- (3) 清水, 岩田, 山本, 室温超伝導を目指した有機分子/金属超薄膜界面, 2D-a06

電子情報通信学会 CPM 研究会, 富山大学工学部, 2003.11.10-11

- (1) 奥山, 金城, 長山, 岩田, 山本, 再蒸発法による C₆₀ 超薄膜ナノ構造, CPM2003-137
- (2) 深井, 榊井, 岩田, 山本, スパッタ法による ReO₃/SrCuO₂ 積層膜の作製, CPM2003-138

2003 MRS FALL MEETING, Hynes Convention Center and Sheraton Boston Hotel, Boston, MA, 2003.12.01-05

- (1) N. Iwata, H. Okuyama, A. Kinjo and H. Yamamoto, One Dimensional Alignment of C₆₀ Molecules Prepared on Thermal Treated Substrates, O3.6

第 26 回フラーレン・ナノチューブ総合シンポジウム 2P-53, 岡崎コンファレンスセンター, 2004.01.07-09.

- (1) 岩田, 長山, 金城, 奥山, 山本, 有機 FET へ向けた C₆₀/CaF₂//Si(111)の作製

NSTI Nanotech(The Nanotechnology Conference and Trade Show), Sheraton Boston Hotel, Boston, MA, 2004.3.07-11

- (1) H. Yamamoto, N. Iwata and Y. Shimizu, Nano-Structured C₆₀-SAM Formed on Ultrathin Au Films/MgO Single Crystal, TU57.01

第 51 回応用物理学関係連合講演会, 東京工科大学, 八王子, 2004. 03.28-31

- (1) 畑, 岩田, 山本, 電子線照射型有機発光素子の発光寿命の検討, 28p-ZR-6
- (2) 山口, 加藤, 高橋, 岩田, 山本, フタロシアニン誘導体混合 LB 膜の高配向化と光吸収特性, 29p-ZR-10
- (3) 榊井, 深井, 岩田, 山本, ReO₃ 薄膜成長に与えるアニール雰囲気の影響, 30p-P16-18
- (4) 佐久間, 清水, 斉藤, 岩田, 山本, Au 超薄膜上 C₆₀ 誘導体自己組織単分子膜の作製と電気伝導特性, 29a-ZF-11 III
- (5) 石川, 橋本, 岩田, 山本, 自由電子レーザーによる 3 次元 C₆₀ ポリマーの合成, 30p-ZW-10
- (6) 大塚, 岩田, 山本, 電気磁気効果薄膜作成とその評価, 30-YF-8

MRS Spring Meeting IUMRS-ICEM 2004, Moscone West, San Francisco, USA, 2004.04.12-16

- (1) H. Okuyama, A. Kinjo, Y. Nagayama, N. Iwata, and H. Yamamoto, Low-Dimensional Nano-Structures of C₆₀ Ultrathin Films by Re-Evaporation Method, T5.11
- (2) H. Yamamoto, N. Iwata, and Y. Shimizu, Resistivity Anomaly Observed at Interfaces of C₆₀ Derivatives self-assembly Monolayer/Ultrathin Au Films, T5.29
- (3) N. Iwata, K. Matsuo, N. Ootsuka, and H. Yamamoto, Preparations and Evaluations of Magnetoelectric Thin Films for Josephson Field Effect Transistor, E3.6

2004 International Symposium on Organic and Inorganic Electronic Materials and Related Nanotechnologies (EM-NANO 2004), Toki Messe, Niigata, Japan, 2004.06.07-10

- (1) H. Hata, N. Iwata, and H. Yamamoto, Electron Beam Excited Light Emission Organic EL Thin Films, P-44
- (2) S. Yamaguchi, K. Katayama, T. Hashimoto, N. Iwata, and H. Yamamoto, Optical Absorption of Highly Oriented Pc Derivatives / Arachidic Acid Mixture LB Films, P-86
- (3) N. Iwata, A. Kinjo, H. Okuyama, and H. Yamamoto, Preparations and Evaluations of C₆₀ Thin Films for Organic-FET, O-A12
- (4) A. Kinjo, H. Okuyama, N. Iwata, and H. Yamamoto, Preparation and Transport Properties of Nano-Structured C₆₀ Thin Films, P-151

- (5) M. Masui, A. Matsumura, N. Iwata, and H. Yamamoto, Synthesis and Transport Properties of $\text{ReO}_3/\text{SrCuO}_2$ Bilayered Films, P-102
- (6) N. Iwata, T. Sakuma, and H. Yamamoto, Resistivity Anomaly Above 100K in C_{60} Derivatives Self-Assembly Monolayer on Ultrathin Au, P85
- (7) T. Ishikawa, R. Hashimoto, N. Iwata, and H. Yamamoto, Synthesis of C_{60} Polymer by Irradiation of Free Electron LASER, P-7
- (8) N. Ootsuka, N. Iwata, and H. Yamamoto, Preparation of Magneto-Electric Oxide / $\text{YBa}_2\text{Cu}_3\text{O}_x$ Thin Films by Sputtering, P-101

第 27 回フラーレン・ナノチューブ総合シンポジウム, 東京大学武田ホール, 2004.07.28-30

- (1) 金城, 奥山, 岩田, 山本, C_{60} 分子のナノ構造作製と電気伝導特性, 3P-15
- (2) 佐久間, 岩田, 山本, Resistivity Anomaly of Self-Assembly Monolayer of C_{60} Derivatives on Ultrathin Au films, 3P-16
- (3) 橋本, 石川, 岩田, 山本, 自由電子レーザー照射による C_{60} ポリマーの合成, 3P-20

電子情報通信学会電子部品・材料研究会, 岩手大学工学部, 2004.08.06

- (1) 奥山, 金城, 浅井, 坂本, 岩田, 山本, 単結晶基板上に形成されたナノ構造フラーレン集合体, CPM2004-45

ELEVENTH ANNUAL INTERNATIONAL CONFERENCE ON COMPOSITES / NANO ENGINEERING (ICCE-11), Hilton-Head Island, South Carolina, USA, 2004.08.08-14

- (1) N. Iwata, A. Kinjo, H. Okuyama, and H. Yamamoto, FABRICATION OF NANO-STRUCTURE BY C_{60} MOLECULES, Session 10a NANO10

Ninth International Conference on Ferrites (ICF9), Cathedral Hill Hotel, San Francisco, California, USA, 2004.08.22-27

- (1) N. Iwata, N. Ootsuka, and H. Yamamoto, Preparation of Magneto-Electric Oxides / $\text{YBa}_2\text{Cu}_3\text{O}_x$ Thin Films, ICF9-HA-6-2004

第 65 回応用物理学学会学術講演会, 東北学院大学, 泉キャンパス, 2004.09.01-04

- (1) 佐久間, 方, 斉藤, 岩田, 山本, C_{60} 誘導体 SAM/Au 超薄膜界面の電気伝導異常, 2a-A-14/I
- (2) 樋口, 中嶋, 若菜, 安達, 岩田, 山本, 田辺, 高温超伝導ランプエッジ型ジョセフソン接合作製における上部電極形成条件の検討, 2a-F-5

European Materials Research Society (E-MRS) 2004 Fall Meeting, Warsaw University of Technology, Warsaw, Poland, 2004.9.6-10

- (1) N. Iwata, M. Masui, A. Muramatsu, and H. Yamamoto, Transport Properties at Interfaces between Conductive Oxide ReO_3 and Cuprate Superconductors, Poster E-9
- (2) N. Iwata, T. Sakuma, T. Fanj, and H. Yamamoto, Resistivity Anomaly Observed in Nano-Structured C_{60} -SAM on Ultrathin Au Films

IUMRS-International Conference in Asia(ICA)2004, Industrial Technology Research Institute(ITRI), Hsinchu, Taiwan, 2004.11.16-18

- (1) H. Yamamoto, N. Iwata, and T. Sakuma, Electronic Transportation Anomaly Observed in Interfaces of Nanostructured C_{60} Monolayers and Ultrathin Au Films (Invited Paper: Symposium A, I-12)

第 15 回日本 MRS 学術シンポジウム, 日本大学理工学部 (駿河台校舎), 2004.12.23-24

- (1) 畑, 岩田, 山本, **Bright Luminescence from Organic EL Thin Films by Electron Beam Irradiation,**
B1-P09-M
- (2) 片山, 山口, 橋本, 岩田, 山本, **Absorption Spectrum of Phthalocyanine Derivatives LB Films,**
B1-P06-M
- (3) 金城, 奥山, 岩田, 山本, **Nano-Structured Alignment of C₆₀,** B1-P02-M
- (4) 橋本, 石川, 岩田, 山本, **Synthesis of C₆₀ Polymer by Irradiation of Free Electron Laser,** Q2-P19-M
- (5) 大塚, 岩田, 山本, **Preparation of Magneto-Electric Oxide / YBa₂Cu₃O_x Thin Films by Sputtering,**
Q2-P21-M

Transport properties of C₆₀ ultra-thin films

Nobuyuki Iwata*, Keigo Mukaimoto, Hiroyuki Imai, Hiroshi Yamamoto

Department of Electronics and Computer Science, College of Science and Technology, Nihon University, 7-24-1 Narashinodai, Funabashi-shi, Chiba 274-8501, Japan

Abstract

We have grown the C₆₀ ultra-thin films on natural mica substrates aiming at nano-scale devices. Whereas, the appearance of the high temperature superconductivity in hole-induced C₆₀ bulk single crystal and CHBr₃ intercalated C₆₀ bulk by the field effect have attracted extensive attention. From the viewpoints of nano-scale devices and superconductivity, we grew single crystal thin films, those were grown on the buffer layer (5 nm thickness) of the C₆₀ ultra-thin films. We concluded that the optimized C₆₀ film was a single crystal with quite-thin thickness on the buffer layer for nano-scale devices and appearance of superconductivity. © 2003 Elsevier Science B.V. All rights reserved.

Keywords: Single crystal; C₆₀ thin film; Buffer layer; Field effect; Superconductivity

1. Introduction

Nano-scale devices are promising for future technologies, for example, organic-based molecules are ordered along 1D and/or 2D [1–3]. In our previous studies, C₆₀ ultra-thin film less than 10 nm thickness has been overspread continuously on mica substrates for nano-scale devices [4].

Whereas, the high-*T_c* superconductivity was observed in bulk C₆₀ and CHBr₃-C₆₀ single crystals, recently, by applying the electric field in order to induce the hole-carriers with a FET configuration [5,6]. The value of the *T_c* is almost same to that of the highest *T_c* of oxides superconductors.

For appearance of the high-*T_c* of the C₆₀ thin films, the films are preferable to be highly oriented, namely single crystal. In this study we reported single crystal C₆₀ thin films and the relation between continuous C₆₀ ultra-thin films, obtained in previous studies, and single crystal C₆₀ thin films.

2. Experimental procedures

We grew C₆₀ thin films in a UHV-MBE system with

*Corresponding author. Tel.: +81-47-469-5457; fax: +81-47-467-9683.

E-mail address: iwata@ecs.cst.nihon-u.ac.jp (N. Iwata).

a background pressure of 1×10^{-8} Torr. A cleaved natural mica substrate was set on the sample holder, where copper foil with 0.01 mm thickness was inserted between the holder and substrate for a better thermal contact and temperature uniformity. Prior to deposition the substrate was prebaked at 400 °C for 60 min in vacuum. The temperature of a substrate was measured by an optical pyrometer. The C₆₀ powder with 99.9% purity was evaporated from PBN crucible in an effusion cell. The cell temperature was varied approximately 310 °C while growing in order to evaporate the specific C₆₀ flux rate by monitoring with a crystal thickness monitor. The growth time was 30 min without exception.

3. Results and discussion

AFM images with $2 \mu\text{m}^2$ are described in Fig. 1 at various temperatures, indicated at upper left of the images. The grains with 50 nm \varnothing were spread in the film surface grown at (a) 40 °C. As the substrate temperature increased, the grain size also increased. In (b) 80 °C, the size of the grains were 150 nm \varnothing , and the part of those grains formed triangle. In (c) 100 °C, the triangle structure was clearly seen, and the size of that was increased with increasing substrate temperature up to 120 °C. Each grain was separated distinctly by the grain-boundaries. Above approximately (d) 120 °C, the triangle-shaped grains began to coalesce and be re-

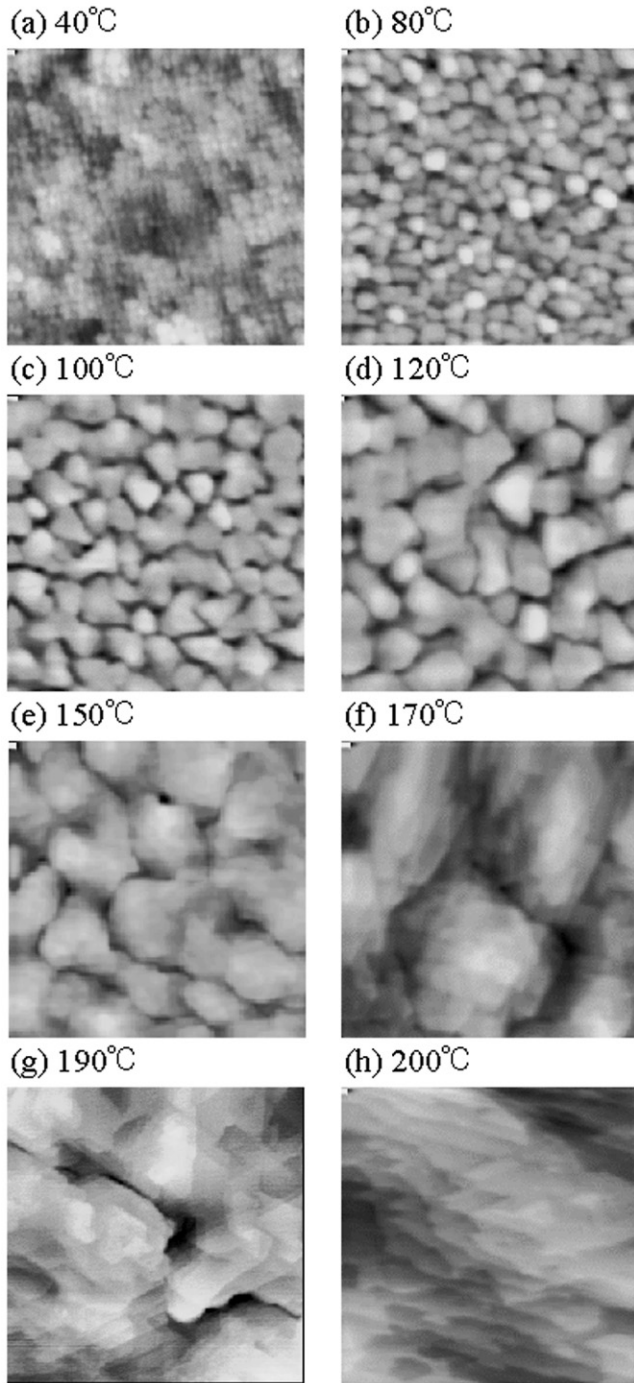


Fig. 1. AFM images with $2 \mu\text{m}^2$ grown at various substrate temperatures. The size of the triangle-shaped grains were increasing with increasing temperature, and then began to coalesce approximately 120°C . Above 170°C , the height of the step was almost same to the lattice spacing of $\text{C}_{60}(1\ 1\ 1)$, 8.16 \AA . In addition to re-orientation in coalesced grains, re-evaporation took place, remarkably, at higher substrate temperature. Consequently 2D films were obtained, demonstrated 60° and 120° facets and larger terraces.

oriented in the coalesced grains. The triangle-shaped grains were no longer present at (e) 150°C . From the result of coalescence and re-orientation of the grains,

steps and terraces structure were observed in (f) 170°C . In (g) 190°C , evident 60° and 120° facets and the terraces with a large size were obtained. The grain boundary from the upper left to lower right was expected from steps of the substrate occurred when the substrate was cleaved. At (h) 200°C , clearer steps and larger terraces were obtained. In some places on a substrate, no film was obtained, indicating that the re-evaporation of C_{60} molecules took place at such a higher substrate temperature. Above (f) 170°C , the height of the step was almost same to that of lattice spacing of $\text{C}_{60}(1\ 1\ 1)$, 8.16 \AA . The result revealed that the direction of the $\text{C}_{60}(1\ 1\ 1)$ was normal to the substrate surface. Above (f) 170°C , the higher the substrate temperature was, the larger terrace size of the top at the each grain was. Increasing of the re-evaporation effect caused the differences of such a surface morphology. Consequently, 2D film was obtained with micrometer-ordered-grains at the higher substrate temperature, where re-evaporation took place, remarkably.

Arrhenius plot of the average radius of the grains is illustrated in Fig. 2 assuming that the shape of grains is circle. The straight line fitted the plots. The value of 0.21 eV as activation energy was estimated from the slope of the straight line. The beautiful fitting indicated that C_{60} crystallized according to the simple model in the whole range of substrate temperatures, and that C_{60} molecules migrated to comfortable positions by overcoming the barrier caused by the van-der-Waals force.

From the XRD results, the full width at half maximum (FWHM) of $\text{C}_{60}(1\ 1\ 1)$ Bragg peak and intensity of the peak are illustrated as a function of substrate temperatures as shown in Fig. 3. The FWHM decreased rapidly up to approximately 100°C , and then showed constant value. As the fluctuation of the lattice spacing, especially perpendicular to the substrate surface, is decreasing, namely as the substrate temperature is increasing, the value of the FWHM for Bragg peak should be decreas-

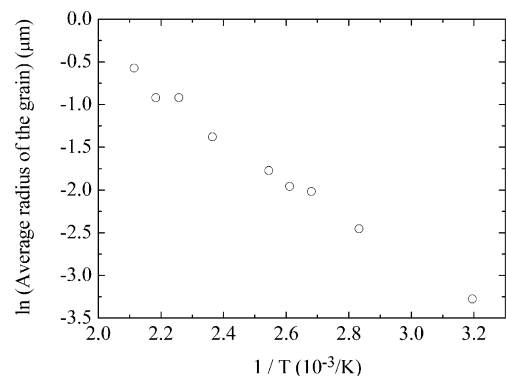


Fig. 2. Arrhenius plot of the average radius of the grains. The straight line fitted well the plots. The value of 0.21 eV as activation energy was estimated.

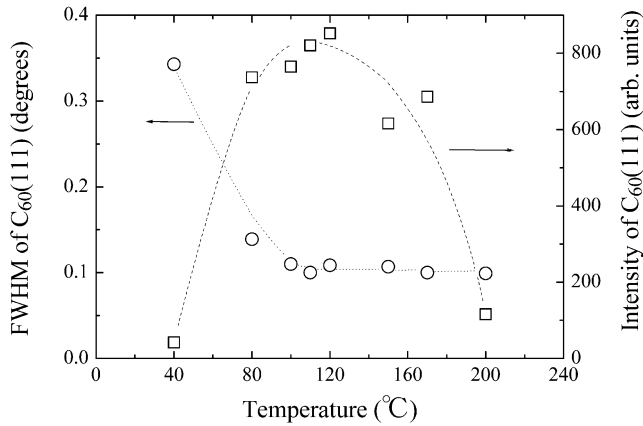


Fig. 3. Substrate temperature dependence of the FWHM of the C₆₀(1 1 1) Bragg peak in left vertical axis and of the intensity of the peak in the right vertical axis.

ing. Whereas, as the film thickness is thinner by the re-evaporation, the value of FWHM becomes larger. Addition of those two effects appeared in the FWHM behavior observed. Same consideration was applicable to the behavior of the intensity of the C₆₀(1 1 1) Bragg peak.

As shown in Fig. 4, the film was grown at 190 °C for 5 min. Substrate surface was clearly seen in the bottom of the image. The 2D islands with thickness of 5 ± 0.5 nm, namely ultra-thin film, were observed around the center of the image. The step and terrace structures appeared in the top of the image. This image indicated that the single crystal C₆₀ thin film grew on the ultra-thin film, namely the buffer layer. The difference of the surface image was expected to attribute to the substrate temperature distribution or the substrate steps indicated by the arrows, which accelerate the nucleation.

Generally, the film growth is affected by substrate surfaces. However, in the case of C₆₀ film growth, the

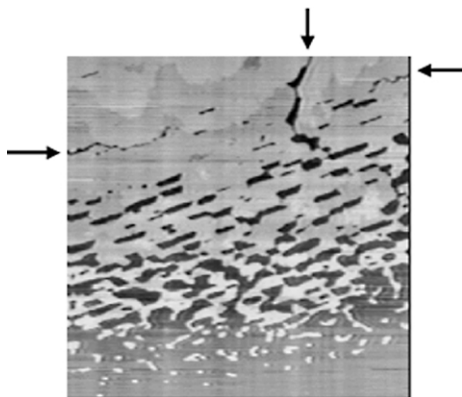


Fig. 4. The AFM image with 5 μm² of the film grown at 190 °C for 5 min. The arrows indicated the grain boundary attributed from substrate steps.

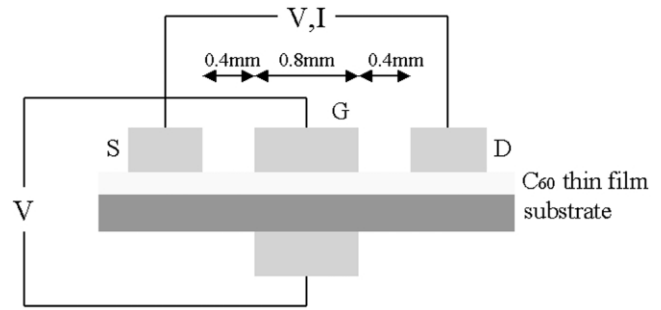


Fig. 5. A schematic view of the specimen configuration for field effect measurements. Tentative electrode sizes are shown in the figure, and the length of those was 5 mm. The thickness of the substrate as a gate insulator layer was 10 μm-order.

substrate effect was expected to be completely reduced due to the existence of the buffer layer. In such a growth condition, film grew according to the simple model, as discussed in Fig. 2, and then close-packed, fcc, structure seemed to be realized.

We concluded that the suitable C₆₀ films for nano-scale devices and FET-superconductivity were single crystal C₆₀ ultra-thin films grown on the buffer layer with 5 nm.

We tried to study the electric field effects of such single crystal C₆₀ thin films on the buffer layer as shown in Fig. 5 with the tentative size. The electrode length was approximately 5 mm. After the deposition of the C₆₀ thin film and Al electrodes (source and drain) in situ, the substrate was exposed to the air and then cleaved with 10 μm-order thickness. Then the substrate was working as a gate insulator. The gate Al electrode was deposited back of the film surface. The resistance between source and drain was too high to measure at room temperature and 77 K. Such a situation did not change when the gate voltage was applied up to ±350 V.

4. Conclusion

Highly oriented single crystal C₆₀ thin films grew on mica substrates with 5 nm buffer layer just below the substrate temperature, where C₆₀ molecules re-evaporated. The direction of the C₆₀(1 1 1) was normal to the substrate surface. Such a film was suitable for nano-scale devices and an appearance of a FET-superconductivity.

Acknowledgments

The authors are grateful for the financial support of the Grant-in-Aid for Scientific Research (No. 12650322).

References

- [1] P.W. Murray, I.M. Brookes, S.A. Haycock, G. Thornton, *Phys. Rev. Lett.* 80 (1998) 988.
- [2] C. Zeng, B. Wang, B. Li, H. Wang, J.G. Hou, *Appl. Phys. Lett.* 79 (2001) 1685.
- [3] M. Böhringer, K. Morgenstern, W.D. Schneider, et al., *Phys. Rev. Lett.* 83 (1999) 324.
- [4] N. Iwata, N. Hashimoto, H. Yamamoto, *Mater. Res. Soc. Jpn.* 26 (2001) 1339.
- [5] J.H. Schon, Ch. Kloc, B. Batlogg, *Nature* 408 (2000) 549.
- [6] J.H. Schon, Ch. Kloc, B. Batlogg, *Science* 293 (2001) 2432.

NOVEL VACUUM SYSTEM FOR IN-SITU CHARACTERIZATION OF FLUORESCENCE PROPERTIES OF THIN FILMS

KOHEI ONOZUKA, NOBUYUKI IWATA and HIROSHI YAMAMOTO

*Department of Electronics & Computer Science, College of Science & Technology,
Nihon University, 7-24-1 Narashinodai, Funabashi-shi, Chiba 274-8501, Japan*
hyama@ecs.cst.nihon-u.ac.jp

We constructed a novel vacuum system in which the cathode luminescence properties of as-prepared films can be measured *in-situ*. It has been observed that the Zn-Ga-O films deposited on 500°C ITO by sputtering emits light with wavelength of about 500 nm from an ultra thin Zn-rich layer formed near film surface. The luminescence induced by irradiation of electrons has also been observed for the first time in the organic bilayered TPD/Alq₃ films prepared in thermal evaporation. Its wavelength blue-shifts by about 120 nm in comparison with the electroluminescence of the same materials. The developed vacuum system is useful to characterize various thin films.

1 Introduction

Recently Flat Panel Displays have been under development because they are expected to surpass the cathode ray tube from the viewpoints of low power consumption, high-speed responses, flexibility and wideness. Organic electroluminescence (EL) or field emission display (FED) has attracted especially much attention as smart interfaces supporting an Information Technology. As component materials for ELD and FED materials of display screens have been developed widely. The more researches and development are, however, required in order to improve the performance of a life, luminous efficiency, and a fine coloring. Then novel tools and techniques for such materials researches are important and have been required.

The purposes of this work are to develop a novel vacuum system for studying fluorescent materials and to explore a novel mechanism of a light emission. We designed a vacuum system in which cathode luminescence properties are measured *in-situ* by irradiating low energy excited electrons without carrying out air exposure for as-prepared films. In the system the two types of fluorescent material systems were adopted and their luminescence properties were investigated. We have studied Zn-Ga-O sputtered films as a typical FED fluorescent material and/or evaporated bilayered organic EL thin films with N, N'-bis (3-methylphenyl) -N, N'-diphenyl-[1,1'-biphenyl]-4,4'-diamine (TPD) and 8-hydroxyquinoline aluminum (Alq₃) in order to evaluate the performance of the constructed vacuum system.

2 Experimental

Figure 1 shows a schematic draw of the vacuum system fabricated in this work. The vacuum system was constructed from two chambers: one is used for film preparations by sputtering, the other for film preparations by thermal evaporation and film measurements on luminescent properties. The chambers connected by a transfer system through gate valves are evacuated independently by turbo molecular pumps.

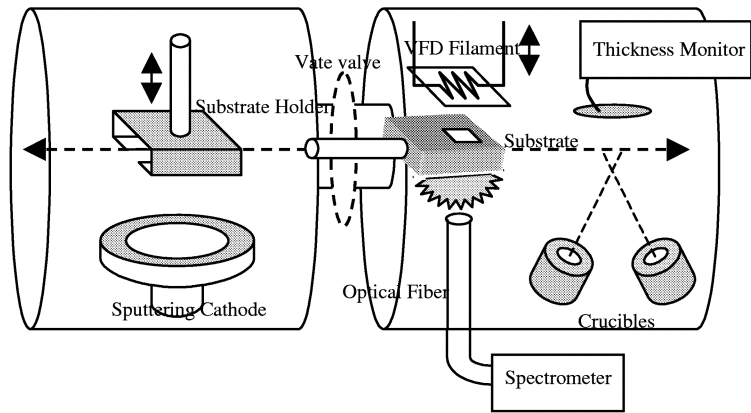


Figure 1 Schematic diagram of the vacuum system.

Thin films of a Zn-Ga-O system were prepared on ITO substrates by RF reactive sputtering. Transferred specimen film was set in a substrate holder which was heated up to the maximum temperature, 600°C. The ZnGa_2O_4 target used was a sintered disk with a diameter of 40 mm. The sputtering conditions were: the sputtering gas of a mixture of Ar and O_2 , the total gas pressure of 10 ~ 20 mTorr, a sputtering power of 100 ~ 200 W, and the deposition rate of about 10 nm / hr.

As the typical organic EL materials TPD (hole transport layers) and Alq_3 (electron transport and luminescent layers) were chosen in order to evaluate the performance of the system. The bilayered films were prepared by a thermal evaporation. The first layer deposited on the ITO glass was TPD and the second layer was Alq_3 . The organic materials were evaporated from the each Al_2O_3 crucible with a W wire-coil. The bilayer was prepared by successively changing the evaporation source. Deposition times were regulated by moved the transfer bar back and forth as a shuttering. The substrate temperature was ambient. The deposition rate of each the layer was about 1.5 ~ 2 Å/sec.

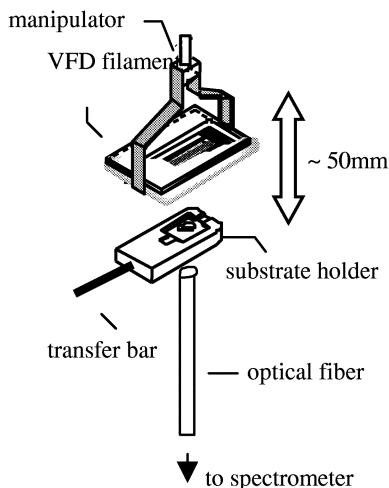


Figure 2 Schematic view of the configuration for the *in-situ* measurement of luminescence.

It is the feature of this system that the peculiar properties of the film can be investigated *in-situ* just after the film deposition. Figure 2 shows the schematic view of the configuration for the *in-situ* measurement of luminescence properties. The vacuum fluorescence device (VFD) filament was used as a thermal electron emission source which could be moved by a manipulator. After transferring the

specimen film to the adequate position, thermal electrons emitted from the filament were accelerated by bias voltage applied to the substrate holder. The luminescence light emitted from the film was guided to a spectrometer (Hamamatsu Photonics K. K., C5966-11) through a hemisphere lens and an optical fiber.

Electron-emission properties of the filament were also measured. For a constant filament current, the emission current density was changed by the acceleration voltage and almost saturated at the maximum $1 \text{ mA} / \text{cm}^2$ in the region of voltage above 200V.

3 Results and Discussion

The Zn-Ga-O film deposited on a 500°C substrate had a compositionally modulated structure. The surface layers of the film were Zn-rich and the inner layers were Ga-rich, while the film deposited on a 50°C substrate was almost stoichiometry [1,2].

A luminescence was observed only in the film deposited at 500°C . Figure 3 shows the spectrum of the cathode luminescence of the film in comparison with that of ZnGa_2O_4 and ZnO powder. The maximum peak of the film luminescence was at about 500 nm and the half width was comparatively wide. The luminescence of the film was similar to that of ZnO powder rather than that of ZnGa_2O_4 powder.

Figure 4 shows the cathode luminescence intensity versus acceleration voltage in the condition of the constant current density. The light emission intensity attained the maximum at about 200 V and decreased as increasing an acceleration voltage. The penetration depth of electron beam at acceleration voltage of 200 V may be very thin, the order of 1 nm. From these results it was concluded that the ultra-thin Zn-rich layers near the surface took an important role for the luminescence. This mechanism is consistent with the similarity in the spectrum of the light emitted from the film and ZnO powder.

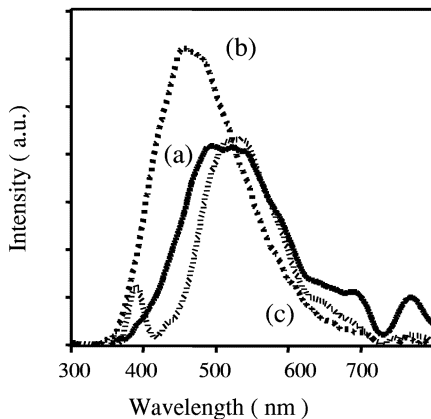


Figure 3 (a) Cathode luminescence spectrum of a Zn-Ga-O film deposited on a 500°C substrate, (b) ZnGa_2O_4 powder and (c) ZnO powder on an ITO.

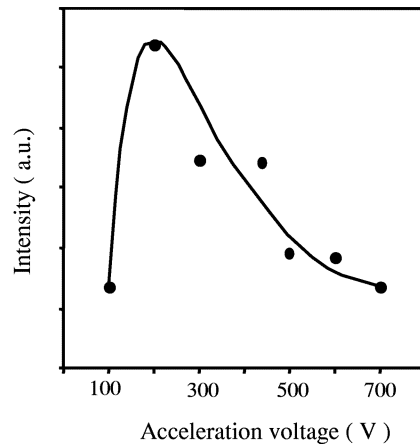


Figure 4 The maximum peak intensity of cathode luminescence versus acceleration voltage.

Figure 5 shows the spectrum of light emissions of the TPD / Alq_3 (20 nm / 20 nm) specimen at acceleration voltage of 210 V. The luminescence by irradiation of a low energy excited electron beam was confirmed for the first time in the organic bilayered film instead of an electroluminescence by a conventional electrode-configuration. The

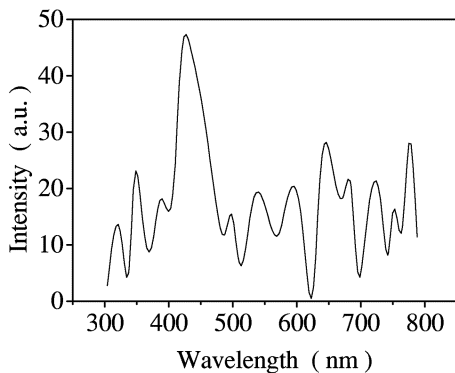


Figure 5 Luminescence spectrum observed in the ITO / TPD / Alq₃ excited by 210 eV electrons.

spectrum of the luminescence clearly revealed the peak at about 430 nm. The reported electroluminescence of TPD / Alq₃[3,4] had the peak at about 550 nm. The newly observed luminescence showed the large blue shift. In the case of the conventional EL electrons injected from the cathode occupied Lowest Unoccupied Molecular Orbital (LUMO) of the luminescence layer. On the other hand, when electrons were injected from thermal electrons emission source, electron penetrated in luminescence layers through from the energy level of vacuum. In this case injected electrons may be captured at energy levels that were higher than

LUMO. Holes were located in the Highest Occupied Molecular Orbital (HOMO) of hole transport layers. We considered that the observed light emission with shorter wavelength was resulted in from the wider energy gap between the electrons and the holes.

When the current density was saturated at acceleration voltages more than 200 V as mentioned above, the intensity of luminescence did not so clearly depend on acceleration voltage. The relaxation and capture mechanism of injected electrons in the film were not understood and should be cleared to explain the blue-shifted luminescence observed in this work.

4 Conclusions

We constructed a novel vacuum system in which the characteristics of luminescence of as-prepared films were measured *in-situ* by irradiating low energy excited electrons without an air exposure of the specimen films. As one of the performances of the system we demonstrated that the cathode luminescence was observed on the surface of Zn-Ga-O sputtered films deposited on 500°C ITO. Also we found for the first time that the bilayered organic electroluminescent films possibly emitted the light with the blue-shifted wavelength compared with the luminescence obtained from the same EL materials system. These newly obtained results suggested that the vacuum system developed here is useful to evaluate the fluorescent properties of as-prepared thin films.

References

1. H. Isogai, Y. Yoshida, and H. Yamamoto, *Trans. of Materials Research Society of Japan*, **24**, 71(1999).
2. H. Isogai, Y. Yoshida, and H. Yamamoto, *Trans. of Materials Research Society of Japan*, **25**, 1139(2000).
3. C. W. Tang, and S. A. VanSlyke, *Appl. Phys. Lett.*, **51**, 913(1987).
4. S. K. Saha, and Y. K. Su, *Journal of Applied Physics*, **89**, 8175(2001).

Transport properties of C60 thin films

Nobuyuki Iwata, Shinji Kuroda, Hiroki Okuyama
and Hiroshi Yamamoto

Presented at the 8th International Conference on Electronic
Materials (IUMRS-ICEM 2002, Xi'an, China, 10–14 June
2002)

Transport properties of C₆₀ thin films

Nobuyuki Iwata, Shinji Kuroda, Hiroki Okuyama and Hiroshi Yamamoto

Department of Electronics & Computer Science, College of Science & Technology,
Nihon University, 7-24-1 Narashinodai, Funabashi-shi, Chiba 274-8501, Japan

We investigated the differences of growth mechanism and electric properties for C₆₀ thin films on natural mica and SrTiO₃ substrates with and without vacuum ultraviolet radiation while growing for the future nano-scale devices. Whereas, electric properties of C₆₀ thin films are also attracted from the point of FET-superconductivity, recently.

Highly oriented epitaxial C₆₀ thin films with *hcp* structure grew at the temperature just below 200 °C, of which surface was 2-dimentionaly flat and showed 60 and 120 degrees facets. At that temperature the surface roughness *Ra* was 0.6 (± 0.2) nm. No apparent differences were detected with and without vacuum ultraviolet radiation. Resistance was too high to detect it with applying the voltage in the FET construction.

Keywords : C₆₀ thin film, mica substrate, epitaxial growth, re-evaporation,

INTRODUCTION

One-dimensional (1D) and/or two-dimensional (2D) ordering of organic-based molecules have attracted the attention for the future nano-scale devices with the self-assembled manner[1-3]. We chose C₆₀ molecules as organic material because of its novel physical and electrical properties. However, electric properties of C₆₀ vary under oxygen atmosphere with light radiation. In this study we investigated the differences of growth mechanism and electric properties for C₆₀ thin films with and without vacuum ultraviolet radiation while growing[4]. Electric properties of C₆₀ thin films are also attracted from the point of FET-superconductivity, recently[5].

EXPERIMENTAL PROCEDURES

We grew C₆₀ thin films in a UHV-MBE system with a background pressure of less than 1×10^{-8} Torr. Main-chamber for film growth and pre-chamber for sample exchange were evacuated by a 2000 l / s diffusion pump and a 220 l / s turbo molecular pump, respectively. The pressure while growing was $2.5 (\pm 0.5) \times 10^{-8}$ Torr.

A cleaved natural mica substrates and SrTiO₃ substrates were set on the sample holder and were prebaked at 400 °C for 60 min and 700 °C for 30 min, respectively. The temperature of a substrate (T_s) was measured by an optical pyrometer through the viewport specially equipped with a ZnSe window.

C₆₀ powder with 99.9 % purity was evaporated from PBN crucible in an effusion cell. The cell temperature was varied while growing in order to evaporate the constant C₆₀ flux rate by thickness monitor. The growth time was 30 min. A 90 nm thick film was deposited on glass substrate at room temperature.

Vacuum ultraviolet light was radiated by a heavy hydrogen lamp (HAMAMATSU : L1835-150W, C3150) at intervals of 65 cm away from substrate.

Grown films were evaluated by XRD (Rigaku : RAD-C) and AFM (Seiko Instruments Inc. SII : SPI3800).

RESULTS AND DISCUSSION

Fig.1(a) and Fig.1(b) showed the 2θ - θ XRD spectrum of C₆₀ thin films grown at 186 °C on mica substrate with vacuum ultraviolet radiation and mica substrate, respectively. Bragg reflections of the C₆₀ *hcp* structure indicated the epitaxial growth on mica substrate. Other reflections were from the substrate confirmed by Fig.1(b). Similar Bragg peaks were obtained at all substrate temperature, independent of the radiation. No film remained at the temperature above 200 °C due to the re-evaporation of C₆₀ molecules. The lattice spacing of C₆₀(002), fitted by Nelson-Riley function, was 0.817 ± 0.001 nm, similar to that of *hcp* bulk, 0.818 nm.

Fig.2 shows the substrate temperature dependence of full width at half maximum, FWHM, of C₆₀(002) Bragg reflection. The FWHM decreased up to 80 °C, and showed

the constant value at the temperature range from 80 °C and 180 °C. Above 180 °C, the value rapidly increased.

Generally, the FWHM of 2θ - θ Bragg reflection depends on the fluctuation of the lattice spacing and the film thickness. As the fluctuation was decreasing with increasing temperature, the FWHM should be reduced, whereas with increasing temperature film thickness became thinner by the re-evaporation, the FWHM should be increasing. These two origins led to the behavior of the FWHM against substrate temperature.

Figs.3 show the AFM images of the C₆₀ thin films grown above 149 °C on mica substrates without vacuum ultraviolet radiation. At all of the images, the step and terraces were clearly observed. With increasing temperature, the terrace width became larger. At 149 °C, Figs.3(a-1,-2), numbers of the grains with spiral growth were observed, indicating the 3D growth mode. At 185 °C, Figs.3(b-1,-2), the separated grains were not obvious, and the spiral growth was obtained in some places on the 2D flat foundation C₆₀ thin film, indicating the 3D growth on 2D. At 197 °C, Figs.3(c-1,-2, and -3), there were no spiral growth, just steps and terraces and 60 and 120 degrees facets appeared. It looked like the 2D growth mode. Above this temperature, no film and no AFM images were obtained due to the re-evaporation.

It was noted that the growth mode looked like changing with increasing temperature. However, above 185 °C, at which re-evaporation was an effective, C₆₀ molecules at the mountaintop of the spiral growth should re-evaporate first. Eventually, the different surface obtained was caused by not the difference of the growth modes but the re-evaporation.

In Fig.4, the line profile of the Fig.3(c-1) is described. Step height of 0.8 nm was perfectly consistent with the lattice spacing of (002) for C₆₀ *hcp* bulk structure.

Temperature dependence of the surface morphology for the films with radiation was almost same to that of the films without radiation. Altogether, it was more difficult to detect the fine images than those of the films grown without radiation, expected from static electricity.

Surface roughness Ra is illustrated as a function of substrate temperature in Fig.5. The Ra decreased linearly with increasing temperature up to 150 °C, and then showed the rapid fall to the lowest point. The rapid decreasing was consistent with the difference of growth modes, demonstrated in the difference of the AFM images between Fig.3(a) and Figs. 3(b,c).

On the SrTiO₃ substrates, no oriented films were obtained from 135 °C to 190 °C without radiation, confirmed by RHEED and AFM.

For electric measurement, we constructed the FET structure. However, the resistance was too high to detect it with applying the voltage.

CONCLUSIONS

As demonstrated in Fig.1(a), Figs.3(c), and Fig.4, highly oriented epitaxial films grew at the temperature just below 200 °C. Growth mode changed from 3D to 3D on 2D above 150 °C, and then 2D surfaces were obtained because of the re-evaporation, see Figs.3 and Fig.5. From the XRD results and AFM images, no apparent difference was detected with and without vacuum ultraviolet radiation.

References

- [1] C. Zeng, B. Wang, B. Li, H. Wang, and J. G. Hou : Appl. Phys. Lett. 79 (2001) 1685.
- [2] P. W. Murray, I. M. Brookes, S. A. Haycock, and G. Thornton : Phys. Rev. Lett. 80 (1998) 988.
- [3] M. Böhrnger, K. Morgenstern, W. D. Schneider, R. Berndt, F. Mauri, A. D. Vita, and R. Car : Phy. Rev. Lett. 83 (1999) 324.
- [4] N. Iwata, K. Mukaimoto, H. Imai and H. Ymamoto : Sur. Coat. Tech. will be published.
- [5] J. H. Schön, C. Kloc, and B. Batlogg : Science **293** (2001) 2432.

Figure captions

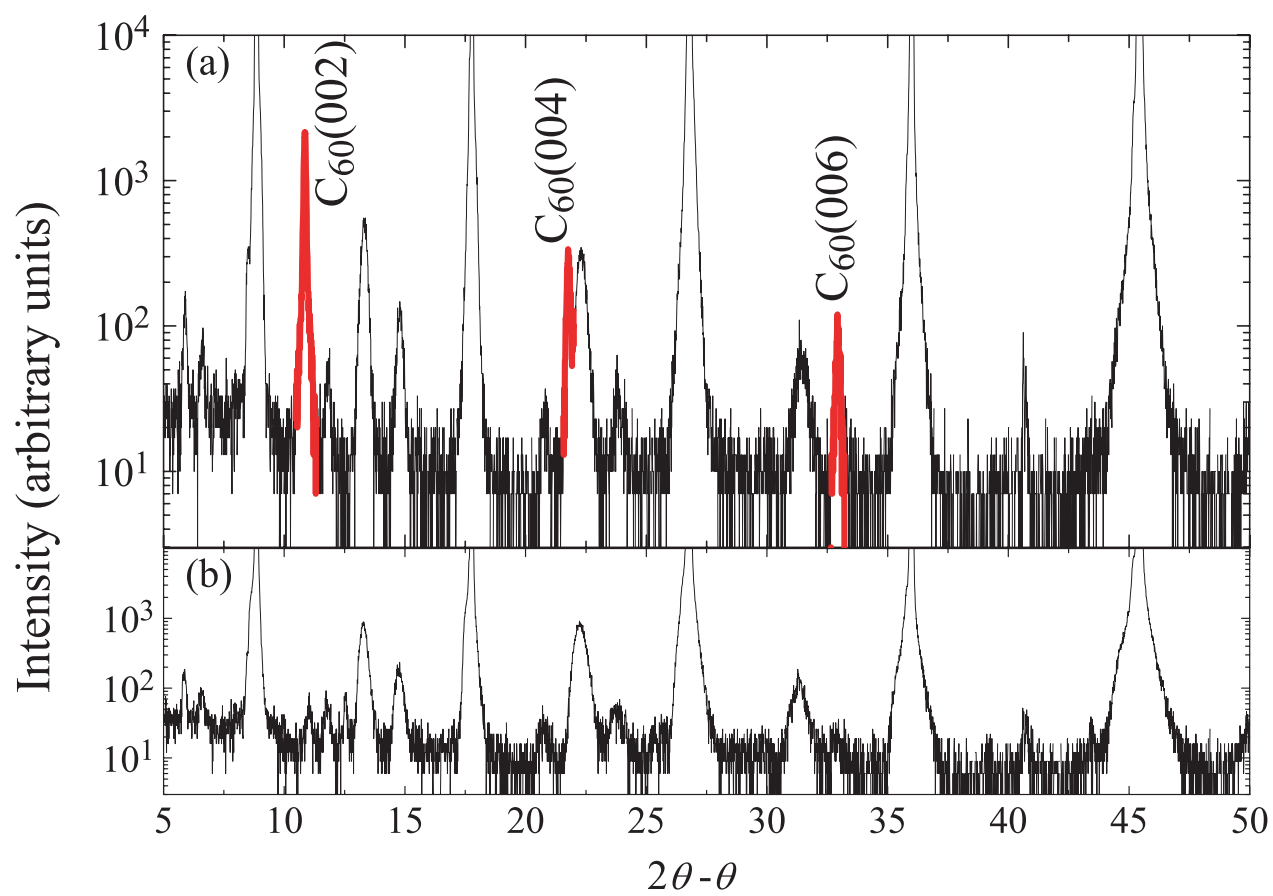
Figure 1 : (a) XRD 2θ - θ spectrum of C_{60} // natural mica substrate grown at 186 °C with vacuum ultraviolet radiation. (b) XRD 2θ - θ spectrum of natural mica substrate.

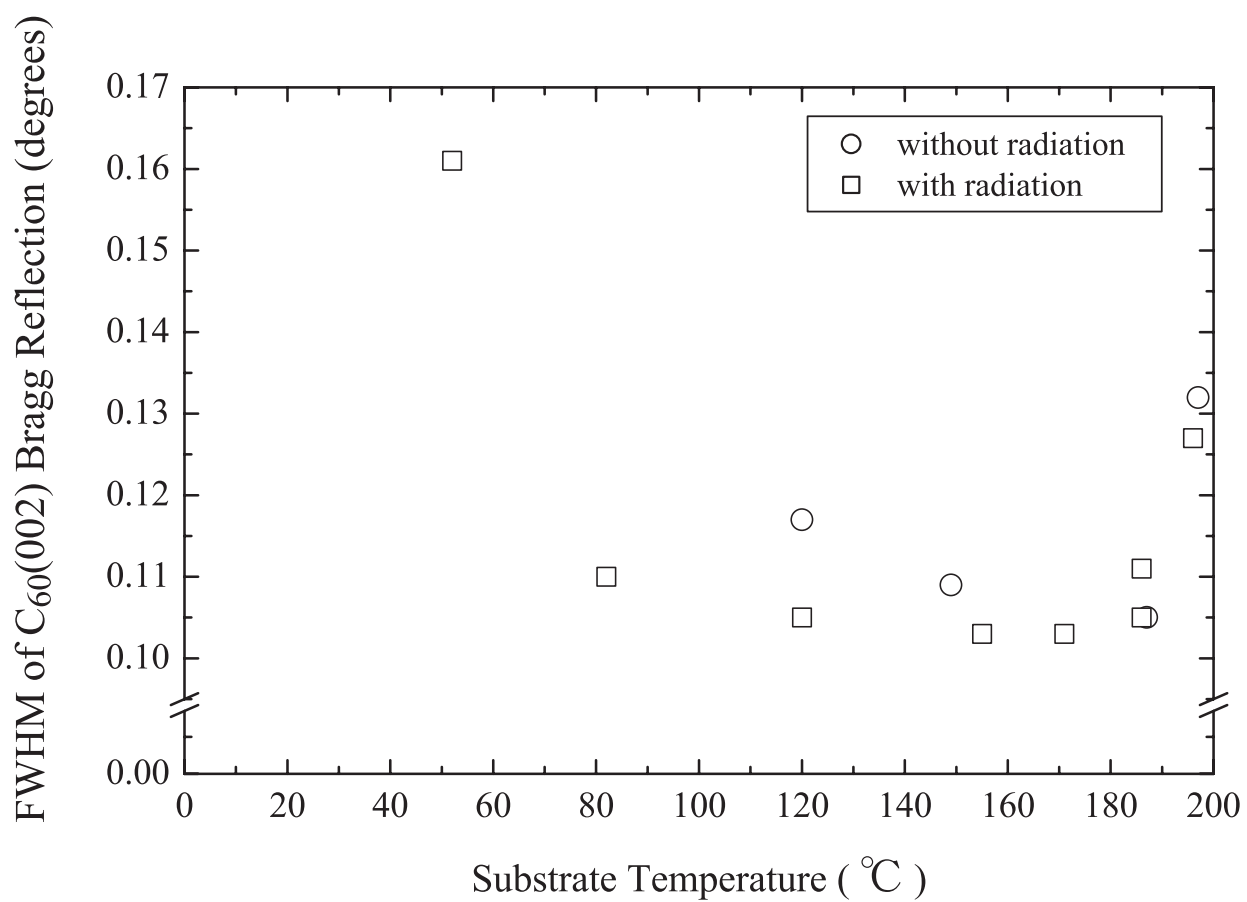
Figure 2 : Substrate temperature dependence of the FWHM of $C_{60}(002)$ Bragg reflection without (○) and with (□) radiation.

Figure 3 : AFM images of C_{60} // natural mica substrate grown above 149 °C without vacuum ultraviolet radiation. The size of the upper images was $2\mu\text{m}^2$ and of the lower images was $5\mu\text{m}^2$.

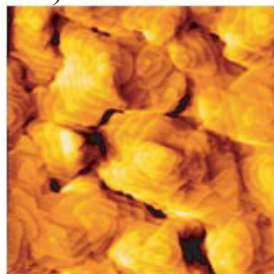
Figure 4 : Line profile of the Fig.3(c-1).

Figure 5 : Substrate temperature dependence of the surface roughness R_a of C_{60} // natural mica substrate without ($2\mu\text{m}^2$: ○, $5\mu\text{m}^2$: ●) and with ($2\mu\text{m}^2$: □, $5\mu\text{m}^2$: ■) radiation.

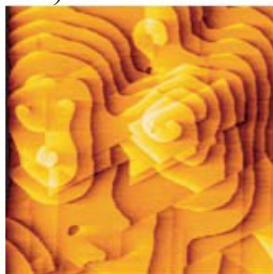




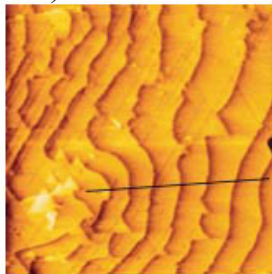
a-1) 149 °C



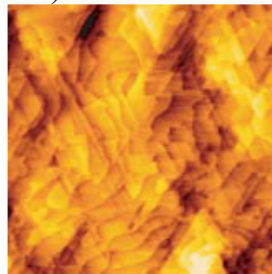
b-1) 185 °C



c-1) 197 °C



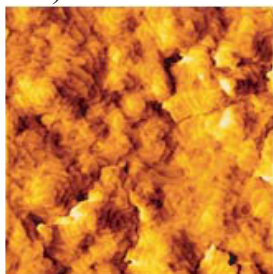
c-3)



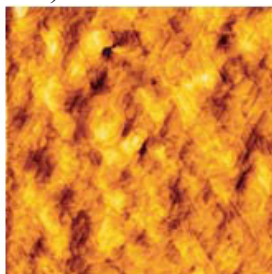
a-2)

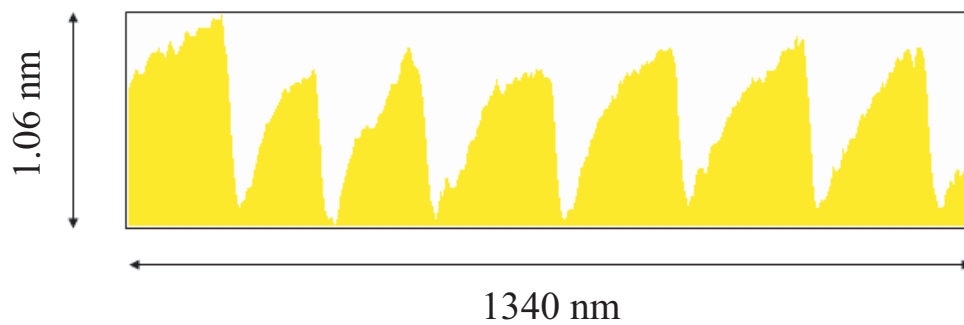


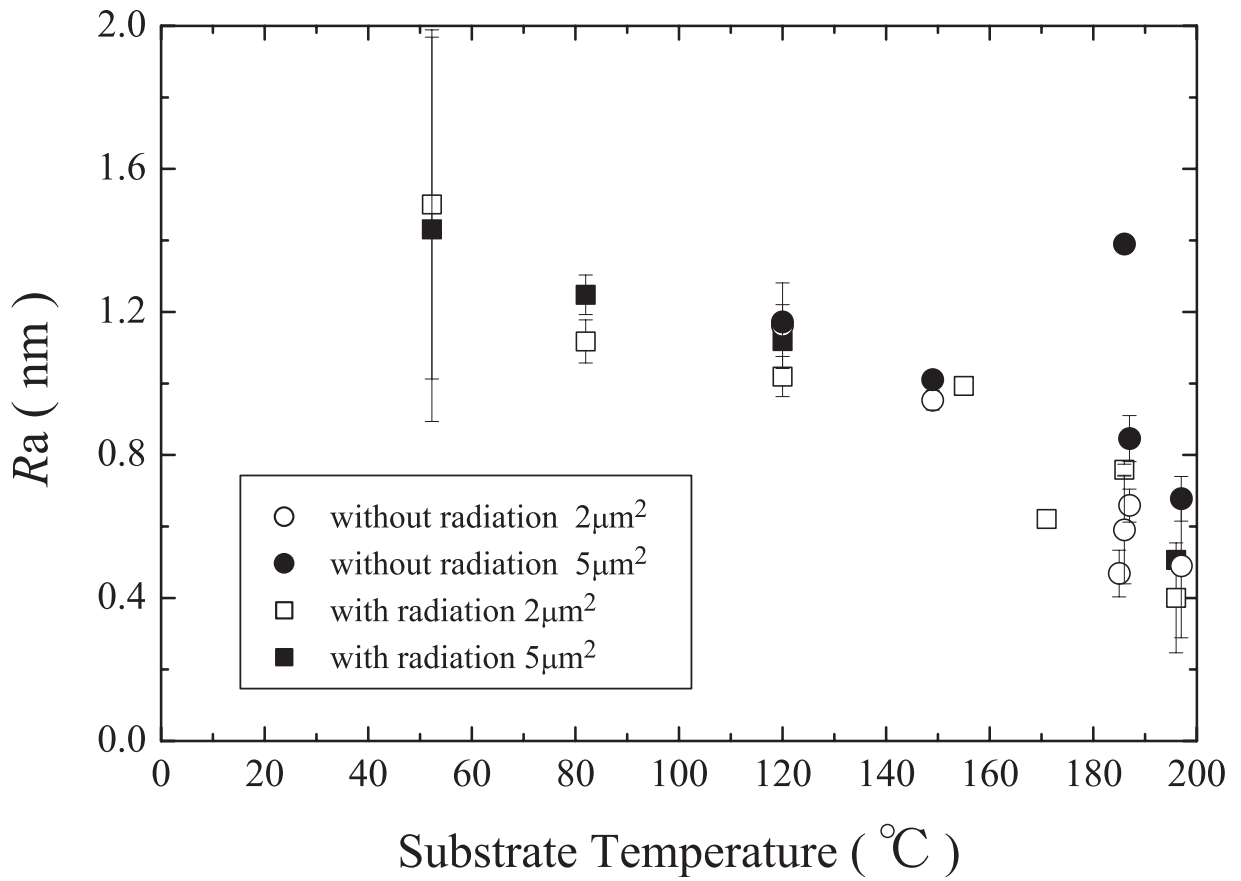
b-2)



c-2)







Low-voltage electron beam excitement luminescence of oxide thin films with multilayered structure

H. Yamamoto*, H. Isogai, Y. Yoshida

College of Science and Technology, Nihon University, Funabashi-shi, Chiba 274-8501, Japan

Abstract

A greenish-blue light emission was observed in sputtered films that were deposited on 773-K substrates from a ZnGa_2O_4 target. The films prepared were amorphous and had a bilayer structure with a compositional modulation formed by self-assembly. The approximately 2-nm surface layers thick were Zn-rich, and the inner layers Ga-rich, in the 40-nm thick film. As the film thickness increased, the strength of the light emission increased and saturated at approximately 60 nm. The strength of the light-emission intensity revealed a maximum at approximately 200 V for the acceleration voltage. In the case of artificial bilayered ZnO/NiO films, continuous ultrathin surface layers were not easily obtained, and no light emissions were observed. © 2001 Elsevier Science B.V. All rights reserved.

Keywords: Cathodeluminescence; Zn–Ga–O; Thin film; Bilayer; Self-assembly

1. Introduction

A field emission display (FED) has been developed as a future emissive display realizing high resolution and low consumption of electric power [1]. Phosphors in the FED need to have a low resistivity, no release of pollutant gas, a highly efficient emission of light, and stabilization of the surface.

Phosphor-type thin films are expected to have several features: little restriction of resistivity, comparatively stable surfaces, and easy synthesis of a multilayered structure [2]. A system of Zn–Ga–O [3] was focussed on as a basic phosphor material in this work. The purpose of the work was to prepare a new type of phosphor thin film and to investigate the possibility for improvement of light-emission efficiency by adopting the multilayered structure.

2. Experimental

Prepared films should be evaluated without exposure

to the atmosphere, because the surfaces of FED phosphor thin films are so sensitive to electron excitation. Thus, a new vacuum system was constructed in order to prepare thin films by sputtering and to analyze in situ cathodeluminescence properties and/or the crystal structure of the film. The details of the vacuum system are described elsewhere [4].

Fig. 1 shows a schematic of the vacuum system used in this work. Zn–Ga–O thin films were prepared by reactive RF sputtering. The targets used were powder mixtures with a diameter of 40 mm. The sputtering gas was a mixture of Ar and O_2 . The total gas pressure was 20 mtorr and the sputtering power was 200 W. The distance between the target and the substrates was approximately 30 mm. Typical deposition rates were very small, approximately 10 nm/h. ITO glass was used as the substrate, which was heated to a maximum of approximately 900 K during deposition.

Measurement of the cathodeluminescent properties of the films was according to the following procedure. After in situ transfer of the specimen film, vacuum fluorescence device filaments were moved towards the film surface by a manipulator. Thermal electrons emitted from the filaments were accelerated by an anode up

* Corresponding author.

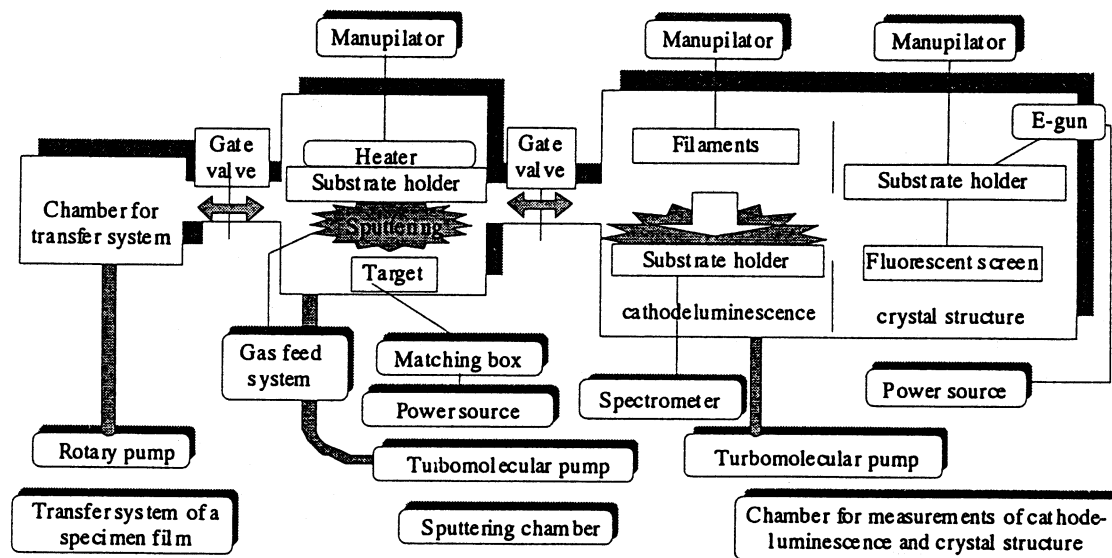


Fig. 1. Schematic diagram of the vacuum system used for sputtering film preparation and in situ measurement of cathodeluminescence.

to 700 V. The cathodeluminescence generated was guided to a spectrometer (Hamamatsu Photonics K. K., C5966-11) through a hemisphere lens of 2 mm diameter and/or an optical fiber.

The film surface structure was studied in situ by reflected high-energy electron diffraction (RHEED) and/or the crystal structure was analyzed by reflected X-ray diffraction (XRD). The depth profile of the film composition was investigated by X-ray photoelectron spectroscopy (XPS).

3. Results and discussion

Thin films of the Zn–Ga–O system were prepared from a ZnGa_2O_4 target. The films appeared to be amorphous from the results of RHEED and/or XRD. The surface of the film was smooth and fine particles of approximately 60 nm were observed.

It was confirmed from the XPS depth profiles that Zn-rich surface layers and Ga-rich inner layers were formed by self-assembly in the films deposited on high-temperature substrates. The thickness of the Zn-rich layer was approximately 2 nm in the case of the ~ 40 -nm thick film. The film deposited on ambient temperature substrates showed almost stoichiometry.

The film deposited on 773-K substrates revealed cathodeluminescence in the form of a greenish-blue light emission. No light emission was, however, observed in the films prepared on low-temperature substrates.

Fig. 2 shows the peak intensities of the light emission as a function of the thickness of the film. Here, the two types of film deposition were investigated. As the film thickness increased, the strength of the light emission increased and saturated at approximately 60 nm in continuously deposited films. The light emission intensity showed, however, a maximum in the film prepared

by four repetitions of 1-h deposition, approximately 10 nm thick.

A typical spectrum of the cathodeluminescence observed is inserted in Fig. 2. The light emission of the film was similar to that of ZnO rather than that of ZnGa_2O_4 . The half-width of the peak was wider than that of ZnO.

Fig. 3 shows the light emission intensity as a function of acceleration voltage V_a . The intensity attained a maximum at approximately 200 V and decreased with increasing V_a . Enhancement of the light emission took place in the bilayered structure.

These results with respect to thickness and/or V_a dependence revealed that the light emissive region was strongly restricted near the surface of the bilayered thin films. The penetration depth of excited electrons and the diffusion region become large with increasing electron energy. The value of $V_a = 200$ V gives a very small penetration depth, of the order of 1 nm. The band gap of surface layers is comparatively smaller than that of inner layers. This is the case of a quantum well potential structure, where carriers involved in light emission are enclosed near the boundary of the bilayers. Thus, an enhancement mechanism for light emission may be available in that region.

On the other hand, an artificial multilayered deposition was also carried out in a ZnO/NiO thin film system with various thickness of ZnO layers. However, no light emissions were observed in the films. Continuous surfaces were not as easily obtained in such artificial bilayered films.

4. Conclusion

Zn–Ga–O thin films and/or bilayered films of

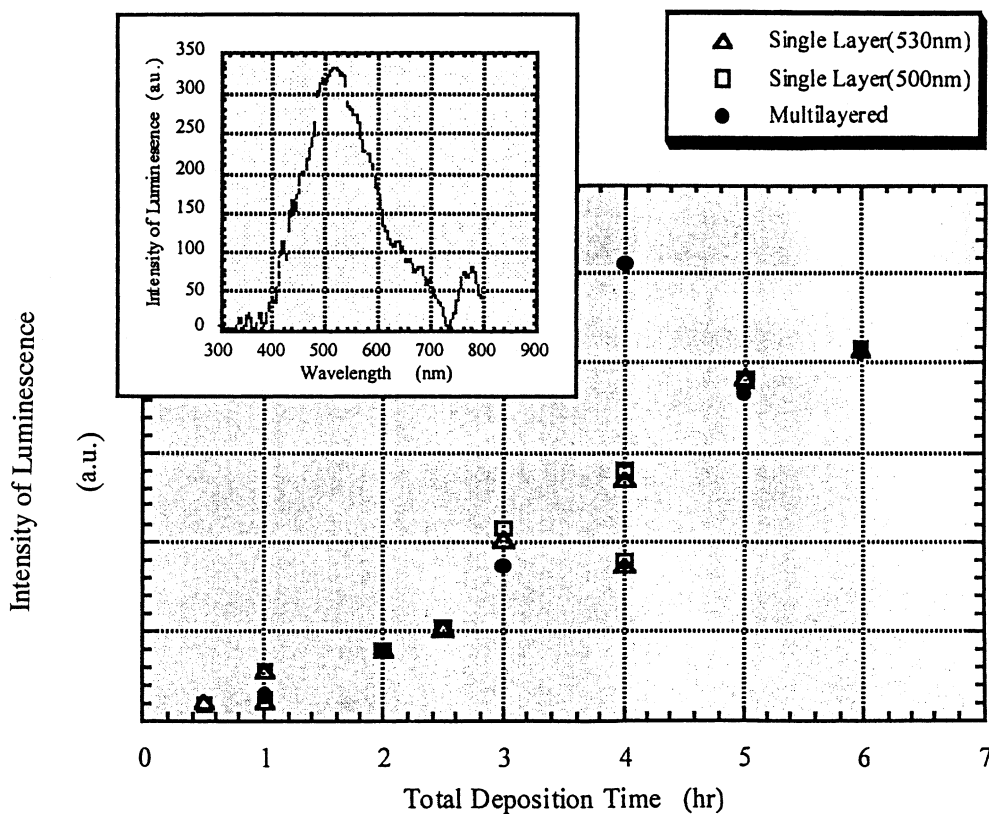


Fig. 2. Intensity of cathodeluminescence peaks of Zn-Ga-O films by the two types of deposition process as a function of deposition time. The inserted figure shows the typical cathodeluminescence spectrum of the film.

ZnO/metal oxide were prepared by sputtering. Only the films deposited on 773-K substrates from the ZnGa_2O_4 target revealed greenish-blue light emissions. The films were amorphous and had a characteristic bilayered structure with a compositional modulation. The approximately 2-nm thick surface layers were Zn-rich, and the inner layers Ga-rich, in the 40-nm thick

film. Low-voltage electron beam excitation luminescence was studied as a function of film thickness and electron acceleration voltage. It was shown that enhancement of the cathodeluminescence took place near the surface of the bilayer structure of ultrathin and continuous surface layers formed by self-assembly.

Acknowledgements

This work was partly supported by a grant from the FUTABA Electronics Memorial Foundation. The authors wish to thank the Advanced Materials Research Center in the College of Science and Technology at Nihon University for help with the physical analyses.

References

- [1] T. Kishino, S. Itoh, Technical Digest, IVMC '95, 30 July–3 August 1995, Portland, OR, (1995) 1.
- [2] I.J. Hsieh, M.S. Feng, K.T. Kudo, P. Lin, J. Electrochem. Soc. 141 (1994) 1617.
- [3] S. Itoh, T. Watanabe, K. Ohtsu, M. Yokoyama, M. Taniguchi, Jpn. J. Appl. Phys. 32 (1993) 3955.
- [4] H. Isogai, Y. Yoshida, H. Yamamoto, Trans. Mater. Res. Soc. Jpn. 24 (1) (1999) 71.

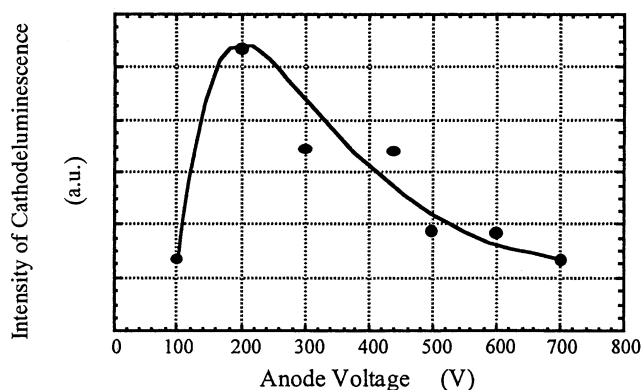


Fig. 3. Intensity of cathodeluminescence of Zn-Ga-O sputtered films, as a function of the anode voltage V_a , for electron excitation.



ELSEVIER

Journal of Physics and Chemistry of Solids 61 (2000) 1047–1050

JOURNAL OF
PHYSICS AND CHEMISTRY
OF SOLIDS

www.elsevier.nl/locate/jpcs

Observation of condensed structure of C₆₀ assembled from solution

S. Ogawa*, H. Furusawa, T. Watanabe, H. Yamamoto

College of Science and Technology, Nihon University, 7-24-1 Narashinodai, Funabashi-shi, Chiba 274-8501, Japan

Abstract

Microscopic needle-like structures with submicron sizes were observed in the films prepared by electrolysis. Macroscopic needle-like structures with few millimeters length were also assembled by an extraction from nonelectrolysis supersaturated toluene solution. The anisotropic activation energy for two kinds of growing surfaces was investigated from the observation of their characteristic structure. Preparation conditions with thermal-equilibrium were thought to be effective to obtain a very long and/or fine assembled structure of C₆₀. Conclusively a huge needle-like C₆₀ was obtained by a very slow extraction. In the sample, ultrafine fibers with a diameter of about 50 nm were observed. © 2000 Elsevier Science Ltd. All rights reserved.

Keywords: C₆₀; Needle-like structure; Ultrafine fiber

1. Introduction

Since the discovery of C₆₀ [1] and the development of mass production of fullerenes [2], they have been widely studied in the field of materials science because of their high feasibilities as a new class of functional materials. Properties of fullerenes often depended on synthesis processes as shown in the results of single crystals or thin films [3]. We have taken notice of a solution process. A few studies have been carried out with respect to the growth mechanism from the solution phase. The purpose of this work is to observe several characteristic structures of C₆₀ assembled from solution and to investigate the growth mode as a function of growing temperature.

The specimens were prepared by two kinds of solution processes. One of the processes was electrolysis, and the other an extraction from a supersaturated solution. The structures of the samples were observed by an electron microscopy, SEM and/or TEM.

2. Assembled metal doped C₆₀ by electrolysis

2.1. Sample preparation

The electrolysis cell was put in a glovebox filled with N₂ gas. The cell had two rooms divided by an ion-exchange membrane. The solution in the working electrode cell was 1.5 mmol/l-C₆₀ toluene. The solution in the counter electrode cell was 0.1 mmol/l-RbClO₄ N,N-dimethylformamide (DMF). A black film was deposited on a silver plate of the working electrode. The temperature of the electrolysis solution was changed from 10 to 60°C. The details of electrolysis conditions appeared elsewhere [4].

2.2. Observation of the assembled structure

Fig. 1 shows the typical SEM photographs of RbC₆₀ compounds obtained by changing the temperature of the electrolysis solution *Te*. At comparatively low *Te*'s, characteristic needle-like particles with the size of a sub-micron were grown. At *Te*'s above 50°C the particles became round.

The growth mode is thought to be reflected in the length ratio along a long axis and a short axis *R* for the needle-like structure. Fig. 2 shows the Alleni plots of the value of *R* as a function of *Te*. From the results, a difference of an effective activation energy ΔE_{act} for the two kinds of growing

* Corresponding author. Tel.: +81-47-469-5457; fax: +81-47-467-9683.

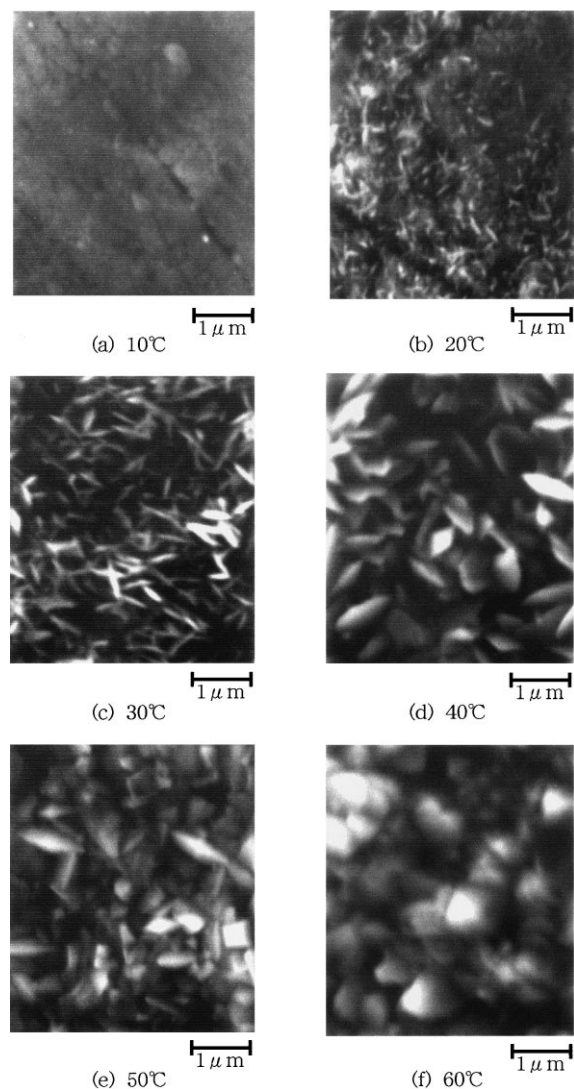


Fig. 1. The SEM photographs of RbC60 compounds obtained by changing the temperature of the electrolysis solution. Tele.

surfaces in the needle-like structure was estimated to be about 35 meV.

3. C60 extracted from the nonelectrolysis solution

3.1. Sample preparation

Assembled structures of C60 were extracted from the toluene solution of C60. The solution of 50 ml was dried in a day and the solution temperature T_{sol} was changed from 20–40°C. Microstructures of the samples were observed by SEM and TEM.

3.2. Observation of the assembled structure

The length of the assembled structure at comparatively low T_{sol} was typically about few millimeters and the diameter was about 1 μm . The shape of the sample became round with increasing T_{sol} as shown in Fig. 3. The Allenius plots of the value of R as a function of T_{sol} is shown in Fig. 4. In this case T_{sol} means a precipitation speed of C60. Then ΔE_{act} was estimated to be about 280 meV, the value of which was fairly larger than that in the electrolysis samples. It was confirmed that a very large anisotropic activation mechanism took place in the thermal-equilibrium for assembled C60 from solution. Conclusively, low-temperature process conditions, namely conditions with thermal-equilibrium, were effective to obtain a long and/or fine needle-like sample.

When the toluene solution was very slowly evaporated in a closed tube, the huge needle-like sample was obtained as shown in Fig. 5. For about 6 months the needle gradually grew at the inner wall of the tube near the surface of the solution. The length and the diameter of the sample attained up to about 20 mm and 100 μm , respectively. The sample was cut into a very thin piece by a focussed ion beam etching technique, and the cross-section of the sample was also observed by TEM. Layered structures with a thickness of about 30 nm were observed. Since a halo electron diffraction pattern was obtained, the assembled C60 was amorphous.

As shown in Fig. 6 an ultrafine fiber with a diameter of about 50 nm was found as the smallest and fundamental structure in the huge needle.

4. Summary

Assembled structures of C60 were obtained by two types of solution processes. As a common mode, a growth of needle-like structures appeared, though the size was quite different, from micrometers to few tens of millimeters. The anisotropic activation energy for the two kinds of growing surfaces was investigated from the results of the observation of the samples. As an experimental proof, a very slow growth of C60 resulted in a huge needle which was composed of ultrafine fibers.

Acknowledgements

This work was partly supported by the Grant-in-Aid for Scientific Research from the Ministry of Education. The authors would like to thank the Advanced Materials Research Center of the College of Science and Technology of Nihon University for usages of physical analyses.

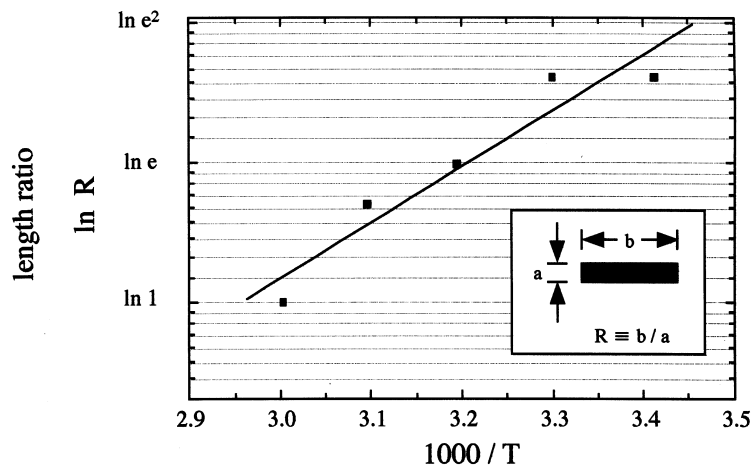


Fig. 2. The logarithms of the length ratio R observed in the needle-like particles prepared by the electrolysis process vs. $1000/T$.

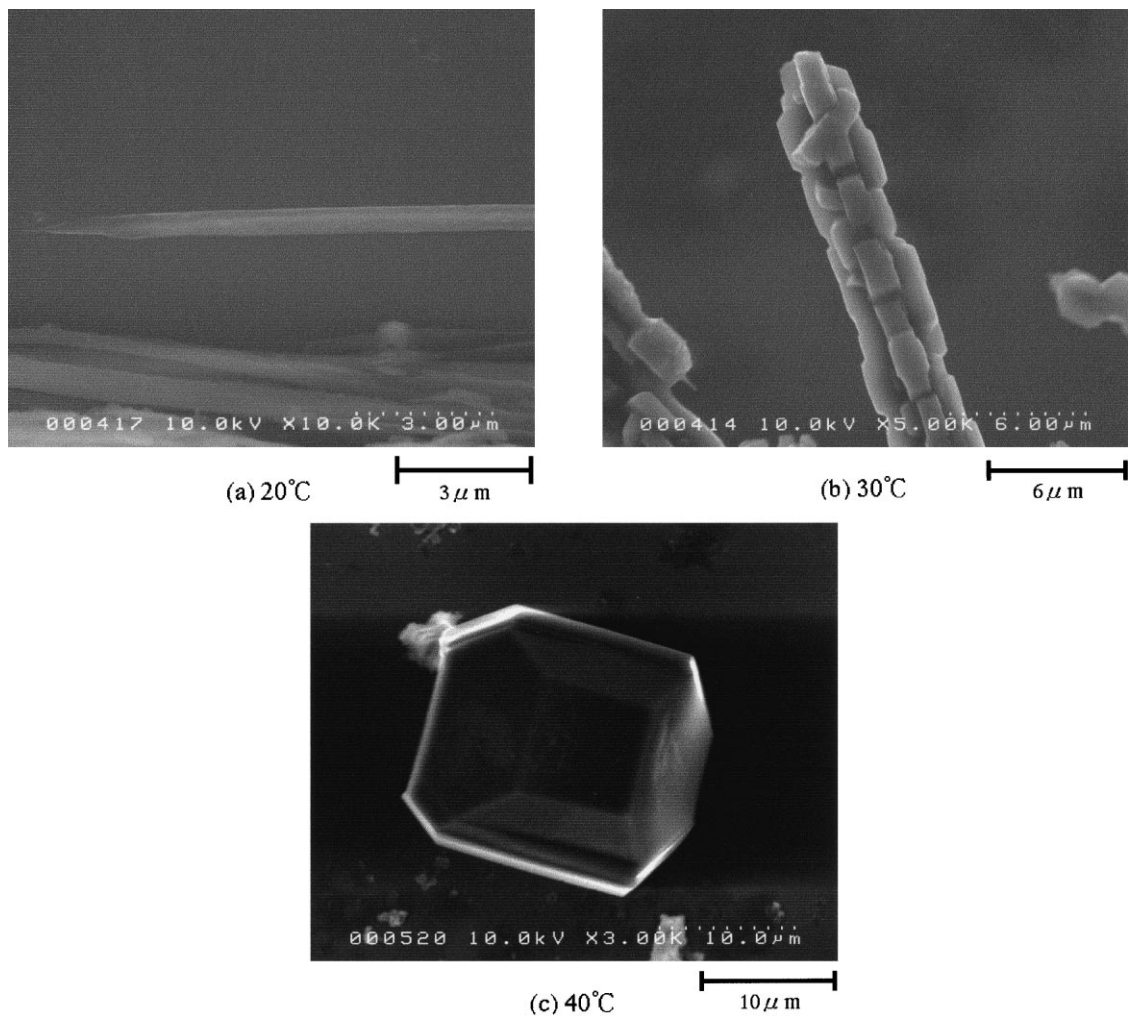


Fig. 3. The SEM photographs of C60 extracted from the supersaturated toluene solution by changing the solution temperature.

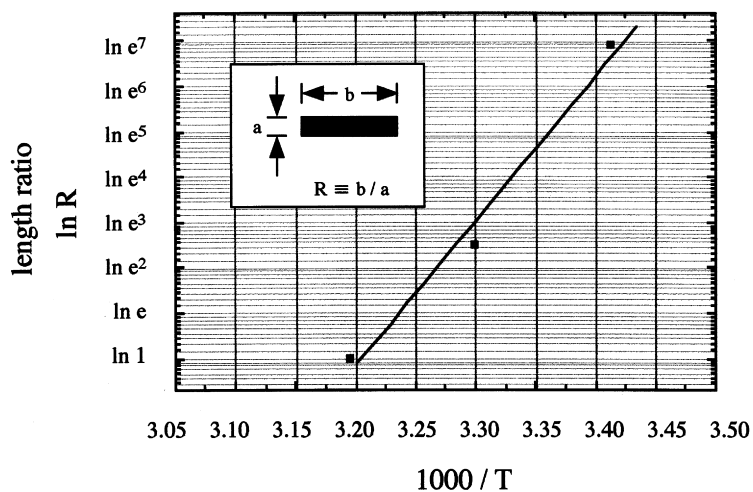


Fig. 4. The logarithms of R of the samples prepared by the nonelectrolysis process vs. $1000/T_{\text{sol}}$.

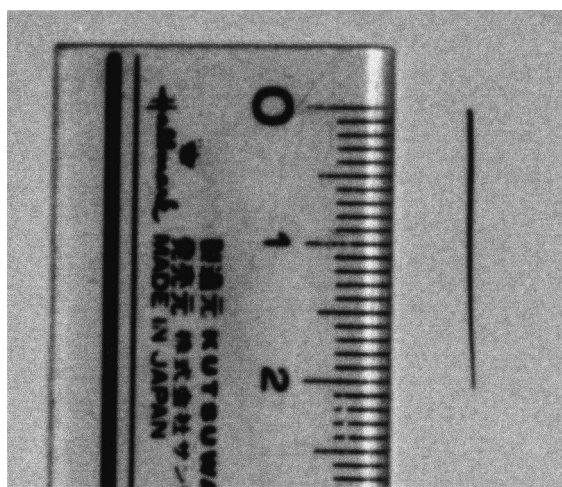


Fig. 5. The huge needle-like sample that was obtained as a result of very slow evaporation of the toluene solution.

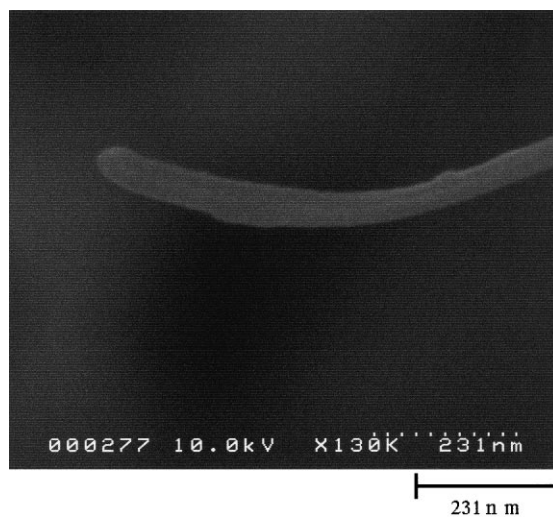


Fig. 6. The SEM photograph of an ultrafine fiber in the huge needle-like sample.

References

- [1] H.W. Kroto, J.R. Heath, S.C. O'Brien, R.F. Curland, R.E. Smalley, *Nature* 318 (1985) 162–163.
- [2] W. Kratschmer, L.D. Lamb, K. Fostiropoulos, D.R. Huffman, *Nature* 347 (1990) 354–358.
- [3] D. Schmicker, S. Schmidt, J.G. Skoffronick, J.P. Toennies, R. Vollmer, *Phys. Rev. B* 44 (1991) 10 995–10 997.
- [4] H. Endo, H. Yamamoto, *Trans. IEE Japan* 118 (1998) 352–357.

Growth and Characterization of Anodic Oxidized Films in Pure Water

Kazunori OHNISHI*, Akira ITO†, Yoshihiro TAKAHASHI and Syunsuke MIYAZAKI

Department of Electronic Engineering, Nihon University, 7-24-1, Narashinodai, Funabashi, Chiba 274-8501, Japan

(Received March 14, 2001; accepted for publication December 12, 2001)

An anodic oxidized film has been deposited in pure water at room temperature. Film thickness increases linearly as a function of total charge during oxidation. High film deposition rate and low surface roughness are obtained by alternately changing the polarity of the applied voltage. The film growth mechanism is discussed and the model of anodic oxidation in pure water is proposed. The HF etching rate and the oxide thickness are reduced by an increase in annealing temperature. Though the electrical characteristics of the anodic oxide film are inferior to those of the film obtained by thermal oxidation, they can be improved by thermal annealing at a temperature of 400°C. [DOI: 10.1143/JJAP.41.1235]

KEYWORDS: silicon dioxide, anodic oxidation, low-temperature process, thermal annealing

1. Introduction

With the progressive shrinking of LSI device size, device and circuit is complexity increasing. The fabrication process is also becoming increasingly difficult. Moreover, there is a great demand to reduce energy consumption on the grounds of preventing global warming and environmental pollution. An oxidation process in VLSI fabrication requires a high temperature of around 1000°C and thermal stress damages the silicon wafer inconspicuously. From this viewpoint, low-temperature processes have been researched. Many low-temperature processes have been proposed to fabricate insulation films on silicon such as plasma deposition, chemical vapor deposition (CVD), photo-CVD,¹⁾ jet vapor deposition (JVD),²⁾ anodic oxidation and so on.

We considered the possibility of applying the electrical effect to the fabrication process of semiconductor devices at low temperatures. The first thing we noted was the occurrence of electrically enhanced oxidation and anodic oxidation on the Si substrate. The effect of the electric field on oxidation has been studied previously.³⁾ Anodic oxidation has been experimentally studied previously as an oxide formation process. Usually, anodic oxidation was carried out with electrolytes such as N methylacetamide (NMA)–KNO₃ or tetrahydrofurfuryl alcohol (THF)–KNO₃.^{4–6)} An anodic oxidized silicon film in pure water was also reported by Dubrovskii *et al.*⁷⁾

Early works on anodic oxidation reported that the etching rate was greater than that of thermal oxides and was changed by impurity solutions and the growth rate was a function of applied voltage in constant current mode.^{5,6)} There is a controversy regarding the oxidation mechanism. Dubrovskii *et al.* proposed the silicon diffusion model in which silicon ions diffused to the oxide–electrode boundary and formed the oxide,⁷⁾ whereas Kraitchman and Oroshnik argued that the oxygen migrates close to the oxide–silicon interface and oxide growth occurs at the interface.⁵⁾

Although the electrical property is improved by high-temperature annealing in He, the oxide films were substantially porous and the electrical property was poor. For these reasons, the use of anodic oxidation was abandoned in integrated circuit fabrication processes.

We intend to study the application of the electrical effect

in the fabrication of integrated circuits at low temperatures. This will contribute to suppressing the energy consumption in VLSI fabrication systems. Here, we report on the experimental method and the characteristics of anodic oxidized silicon dioxide films grown in pure water at room temperature as a possible oxidation process at a low temperature. We discuss the electric characteristics and growth mechanism. We clarify that the surface roughness of the oxide is improved by alternately changing the polarity of the applied voltage and that the oxide thickness is not increased by the applied voltage, but increases with the total charge flowing between electrodes during oxidation. The electrical characteristic is improved by annealing over 400°C after oxidation.

2. Experimental

Samples used in our experiments were fabricated as shown in Fig. 1. Wafers used in this experiments were n-type and p-type silicon wafers of $\langle 100 \rangle$ plane and their corresponding resistivities were 3–5 $\Omega\cdot\text{cm}$ and 0.8–1.2 $\Omega\cdot\text{cm}$. The wafers were cleaned by the standard RCA cleaning method. Anodic oxidation was carried out in pure water with resistivity of 16 M $\Omega\cdot\text{cm}$ at 20°C. After oxidation, wafers were annealed in nitrogen atmosphere at various appropriate temperatures. A reference sample was prepared by thermal oxidation at 1045°C in dry oxygen and annealed at the same temperature in nitrogen. Film thickness was

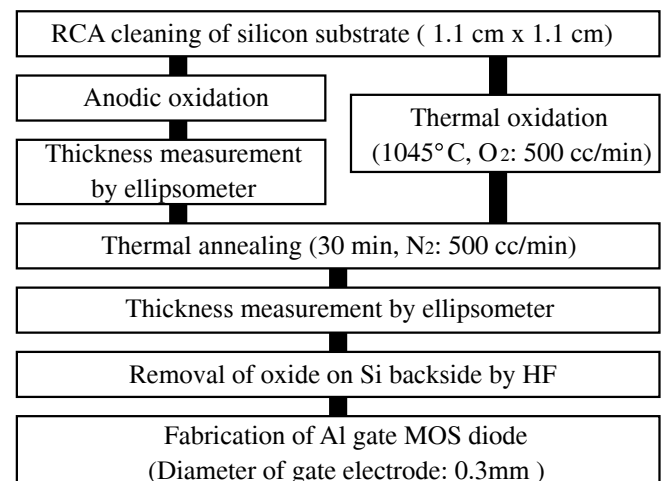


Fig. 1. Sample preparation process flow.

*E-mail: ohnishi@ecs.cst.nihon-u.ac.jp

†Present address: Sanken Electric Co., Ltd., 3-6-3 Kitano, Niiza, Saitama 352-0003, Japan.

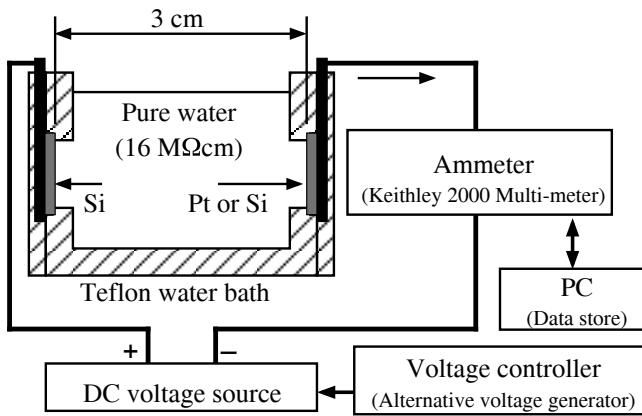


Fig. 2. Anodic oxidation experimental system.

measured by the ellipsometry method. The film composition was analyzed by X-ray photoelectron spectroscopy. Electrical properties were measured using MOS structures with aluminum electrodes. Anodic oxidation was carried out in pure water with the application of a constant voltage across the silicon wafer anode and the other electrode of platinum or silicon, as shown in Fig. 2. The distance between the electrodes was 3 cm, and anodic oxidation was carried out with a constant DC voltage or by alternately changing the

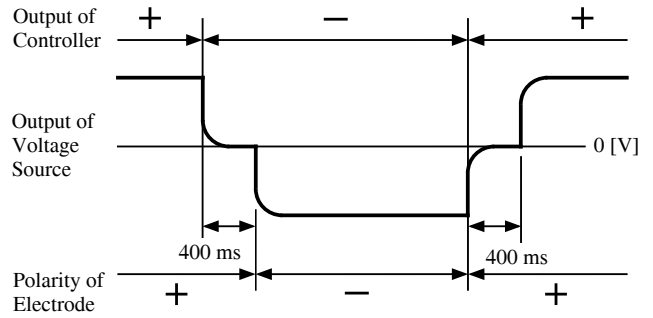


Fig. 3. Time chart of alternately changed polarity of voltage (AC).

polarity of the voltage (AC). We used the period of 60 s and the duty ratio of 0.5 for the AC voltage source. Figure 3 is a time chart of applied voltage when the polarity changes alternately. The current flow during anodic oxidation was monitored and integrated to calculate the total charge during oxidation. Silicon substrates were cut to a 1.1 cm square size, and the anodic oxidation window was 1 cm square.

3. Experimental Results

We measured distributions of the thickness of both samples fabricated with DC and AC voltages. Figure 4 shows profiles of oxide films in this experiment. Figures 4(a)

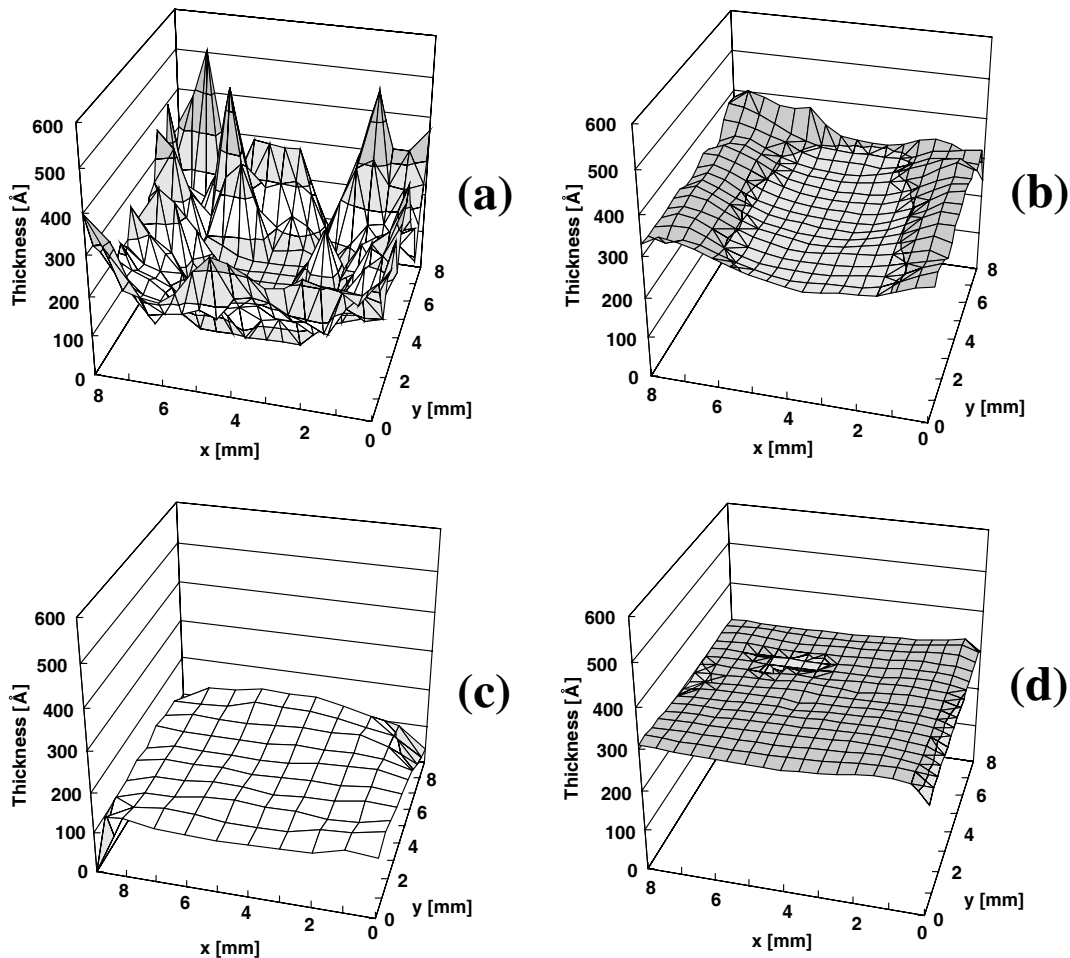


Fig. 4. Profile of oxide thickness. (a) on n-Si with 300 V DC (b) on p-Si with 300 V DC (c) on n-Si with 300 V AC (d) on p-Si with 300 V AC.

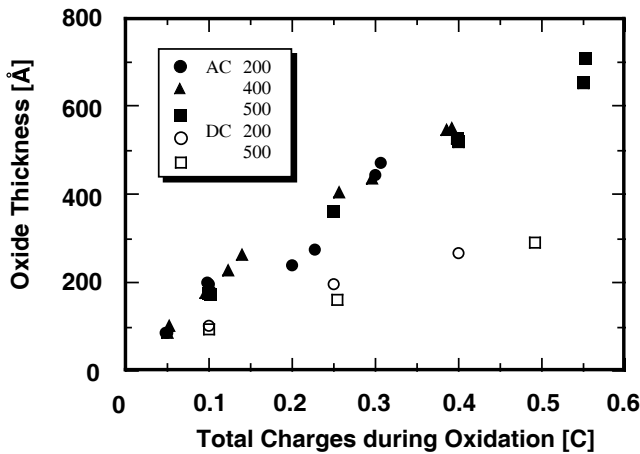


Fig. 5. Film thickness vs total charges during anodic oxidation on p-type (100) 3–5 Ω -cm Si at 20°C.

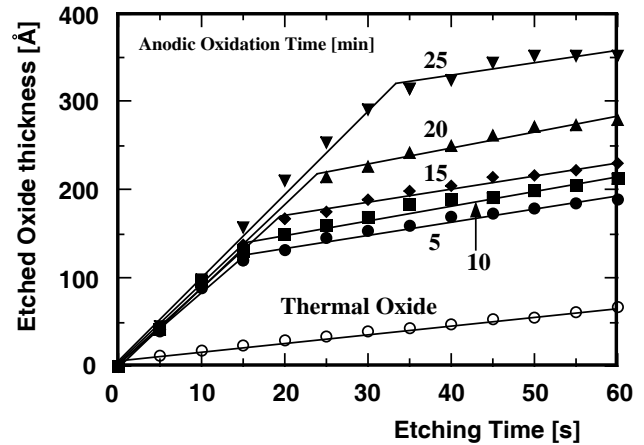


Fig. 6. Etched oxide thickness vs etching time for different anodic oxidation times.

and 4(b) show thickness distributions of the oxide film on the n-type and p-type silicon substrates when the voltage was 300 V DC. Figures 4(c) and 4(d) show distributions of the oxide thickness when the applied voltage changed polarity as shown in Fig. 3. The oxide on the n-type substrate was thinner than that on the p-type substrate and randomly distributed, but it was improved upon oxidation with an applied AC voltage as shown in Fig. 4(c). Figure 5 shows the oxide thickness on the p-type silicon substrate against the total charge flowing in the system during oxidation for different applied voltages. This figure shows that the oxide film thickness linearly increased with total charges during oxidation and the oxide obtained with AC voltage is thicker than that obtained with DC voltage. The oxide thickness as a function of total charges flowing during oxidation with AC voltage is twice that with DC voltage. The composition of the anodic oxidized film in our experiment was analyzed by X-ray photoelectron spectroscopy; it was stoichiometric SiO_2 , the same as the thermal oxide formed at 1045°C.

We estimated the etching rate of thermal oxide and anodic oxide films in order to compare the quality. The thermal oxide film of 30 nm thickness was grown on a p-type silicon substrate at a temperature of 1045°C and then it was reoxidized by anodic oxidation with 300 V AC for 5–25 min. These samples were etched by a solution of $\text{HF}(48\%) : \text{H}_2\text{O} = 1 : 50$ at room temperature. Figure 6 shows the etched oxide thickness against etching time for various anodic oxidation times. The region of high-etching rate at an early stage is predominantly of anodic oxide and the region of low-etching rate a later stage is predominantly thermal oxide being slightly affected by anodic oxidation. This result reveals that the density of anodic oxide is lower than that of thermal oxide as reported previously. The etching rate of the thermal oxide film is 1 Å/s, and 8–9 Å/s for the reoxidized film by anodic oxidation. It is confirmed that the etching rate of the oxide film fabricated by anodic oxidation (300 V AC) on the silicon substrate is 25 Å/s, and the rate of the film grown with DC voltage is higher than that with AC voltage.

The refractive index of the anodic oxide film was around 1.45 for films thicker than 200 Å, however it ranged from 1.3 to 1.4 for films thinner than 100 Å. The dielectric constants

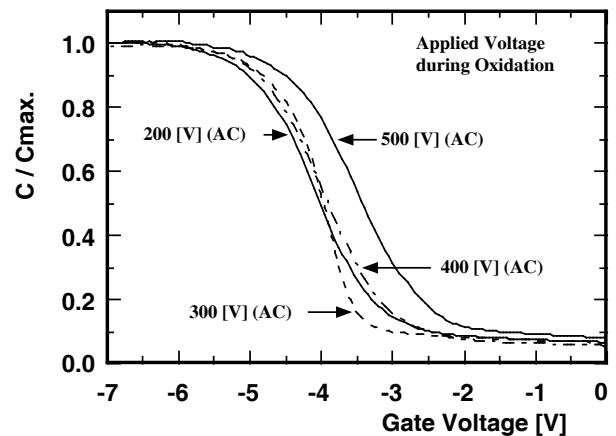


Fig. 7. C - V curves of MOS structures with anodic oxide fabricated at different voltages.

were determined using the thickness measured by ellipsometry and the capacitance measured under accumulation condition. The estimated dielectric constant was between 4 and 7 and it was higher than that of the thermal oxide.

The electrical characteristics are analyzed from high-frequency C - V and I - V characteristics. Figure 7 shows the C - V curves for different anodic voltages and Fig. 8 shows the density of Si/SiO₂ interface states evaluated by the Terman method. Densities of fixed positive charge in the oxide are evaluated by flat-band voltages, and 4.5 – $4.7 \times 10^{12} \text{ cm}^{-2}$ and $3.2 \times 10^{12} \text{ cm}^{-2}$ are obtained when the applied voltages during oxidation are 200–400 V and 500 V (AC), respectively.

Anodic oxidized films were annealed in nitrogen atmosphere at various temperatures. The etching rate and also thickness decrease as the temperature increases as shown in Figs. 9 and 10.

Electrical characteristics are improved by high-temperature annealing. Figure 11 shows the C - V curve of a MOS structure annealed in nitrogen atmosphere at 400°C for 30 min. The anodic oxidized film is fabricated with 300 V AC and the total charge during oxidation is 0.1 C. The density of fixed positive charge is $4.3 \times 10^{11} \text{ cm}^{-2}$. Figure 12 shows the density of Si-SiO₂ interface states of the same

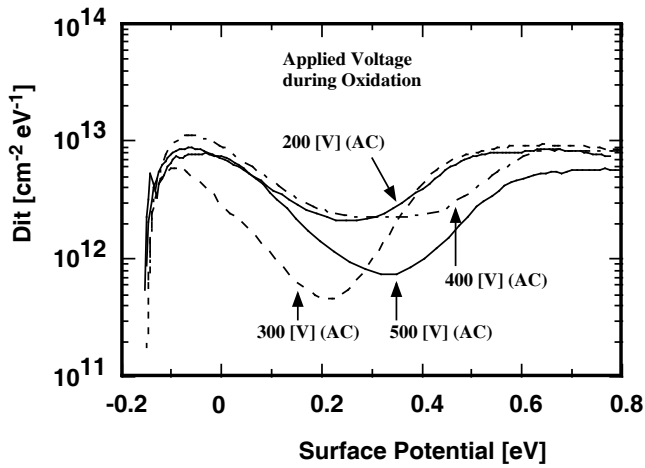


Fig. 8. Interface states density vs surface potential evaluated from $C-V$ curves in Fig. 7.

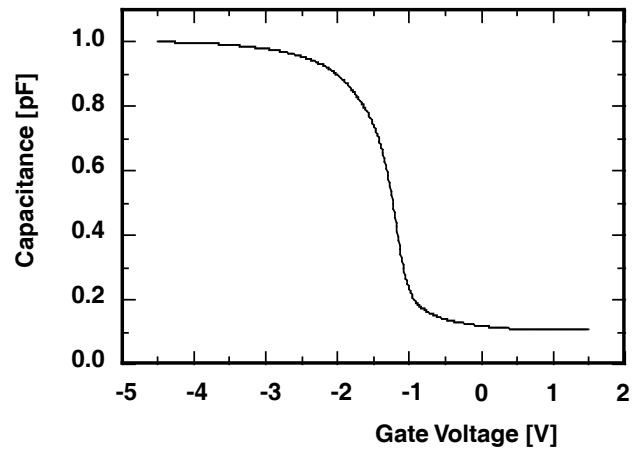


Fig. 11. $C-V$ characteristic of a MOS structure after annealing at 400°C for 30 min. Anodic oxide is fabricated at 300 V AC, total charge is 0.1 C.

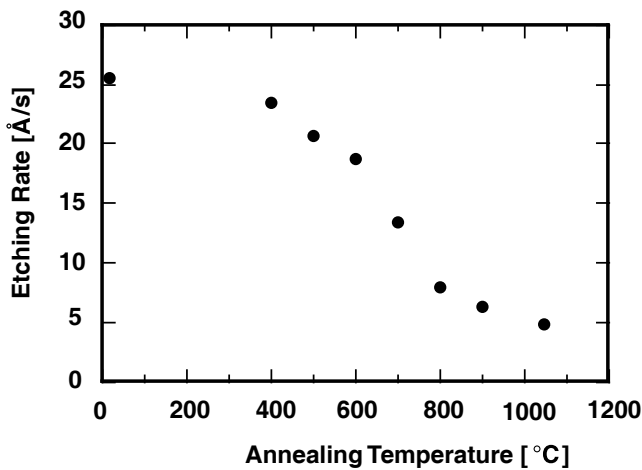


Fig. 9. Etching rate of anodic oxide after annealing in N_2 atmosphere for 30 min at different temperature. Anodic oxidized with DC voltage and total charge is 1 C.

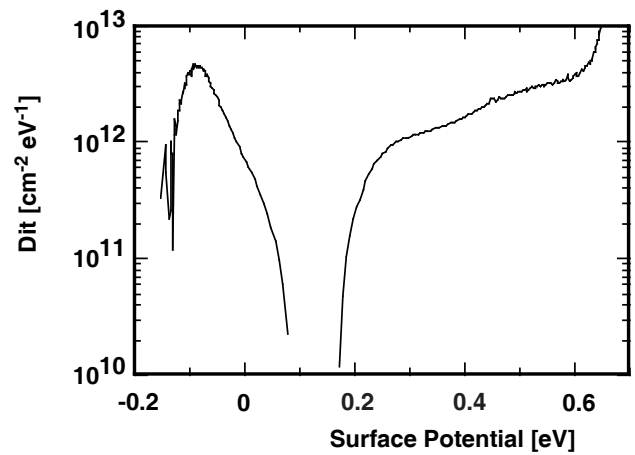


Fig. 12. Interface states density vs surface potential evaluated from $C-V$ characteristic of Fig. 11.

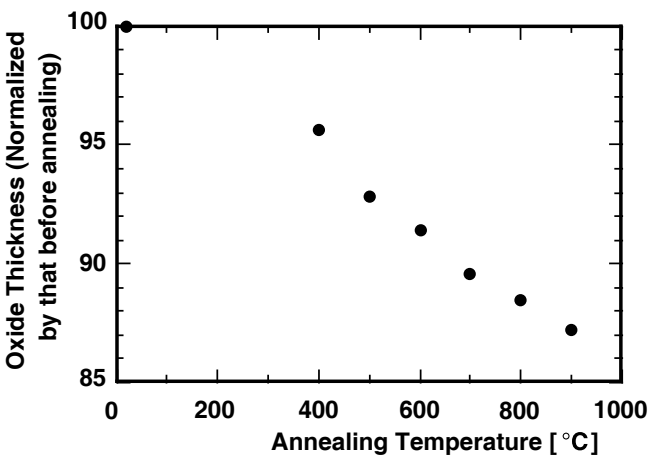


Fig. 10. Thickness change at different annealing temperature in nitrogen atmosphere for 30 min. Anodic oxidation condition is the same as in Fig. 9.

structure.

4. Discussions

In this paper, we explain our experimental results of anodic oxidation on the silicon substrate in pure water at room temperature. The growth rate of the oxide film on the n-type substrate is smaller than that of the oxide film on the p-type substrate and SiO_2 grows only under the condition that the voltage of the silicon wafer is positive. The thickness of the oxide film increases as the total charge during oxidation progresses; this result differs from that of Dubrovskii's experiment. Oxidation by alternately changing the voltage polarity makes the surface roughness decrease. The oxidation rate on the p-type substrate is larger than that on the n-type substrate and moreover, the surface flatness of the anodic oxide film on the n-type substrate is poorer than that on the p-type substrate. When the electrode polarity changes alternately, the oxide growth rate is twice that of the case of single polarity and the surface roughness of the oxide film on the n-type substrate is improved.

From these experimental results, we will consider the anodic oxidation mechanism as follows. A water molecule has a small dipole moment. Electrons of hydrogen atoms take positions close to the oxygen atom side. A hydrogen

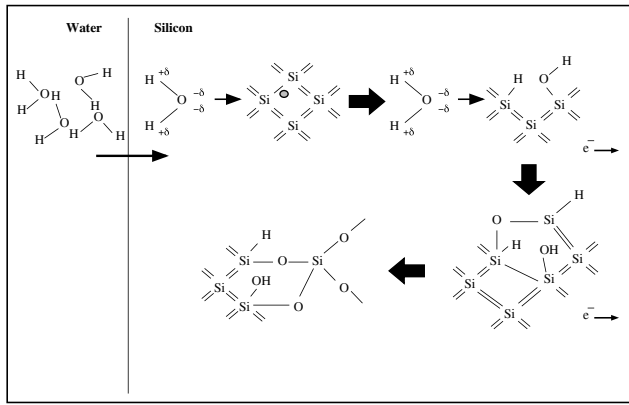


Fig. 13. Proposed model of anodic oxidation in pure water.

atom is slightly positively charged, $+\delta$, and the oxygen of a water molecule is slightly negatively charged, -2δ as shown in Fig. 13. When the silicon wafer is biased positive against a cathode, positive charges exist at the water–Si interface. Oxygen of a water molecule is directed toward the positively charged Si–water interface as shown in Fig. 13.⁸⁾ The water molecule drifts and/or diffuses into the silicon bulk, and hydrogen is dissociated from H_2O . This hydrogen is highly activated and reacts with Si=Si bonds and/or dangling bonds forming SiH and also breaks the covalent bond of Si=Si. The oxygen-hydrogen pair atom combines with Si and forms SiOH.

When a negative bias is applied to the silicon substrate, the hydrogen of a water molecule is directed toward the Si–water interface and the water molecule is dissociated to hydrogen and hydroxyl by reacting with electrons from the negative electrode.⁵⁾ Hydrogen drifts and/or diffuses into the silicon bulk and reacts with Si=Si forming Si–H. OH drifts out to the water. Another possible mechanism is that OH and H in the water are dissociated from a water molecule and H drifts and/or diffuses into the silicon bulk and forms Si–H and/or is positioned at an interstitial site. The hydrogen diffuses deeply into the inner space of the silicon bulk due to a large diffusion constant.

When the polarity of the supplied voltage to the silicon substrate is changed from negative to positive, electrons move from the Si–metal interface to the water–Silicon interface and the distributed ions at the interface are neutralized by the electrons. Moreover, activated hydrogen remaining in the oxide approaches the water–Si interface. The hydrogen distributed in the silicon bulk breaks the Si=Si bond and forms Si–H, and OH from the water–Si interface forms the Si–O and SiO_2 as shown in Fig. 14. Thus the oxidation rate against total charges during oxidation in case of AC voltage is roughly twice that with DC voltage as shown in Fig. 5. In the case of the p-substrate, holes accumulate sharply at the interface as shown in Fig. 15. Meanwhile, in the case of the n-substrate, donor ions form a depletion layer, holes (minority carrier) are present at the interface as shown in Fig. 16 and a depletion layer restricts the growth rate.

The growth rate difference between SiO_2 on the n-type substrate and on the p-type substrate is considered as follows. In case of the p-type silicon substrate, positive

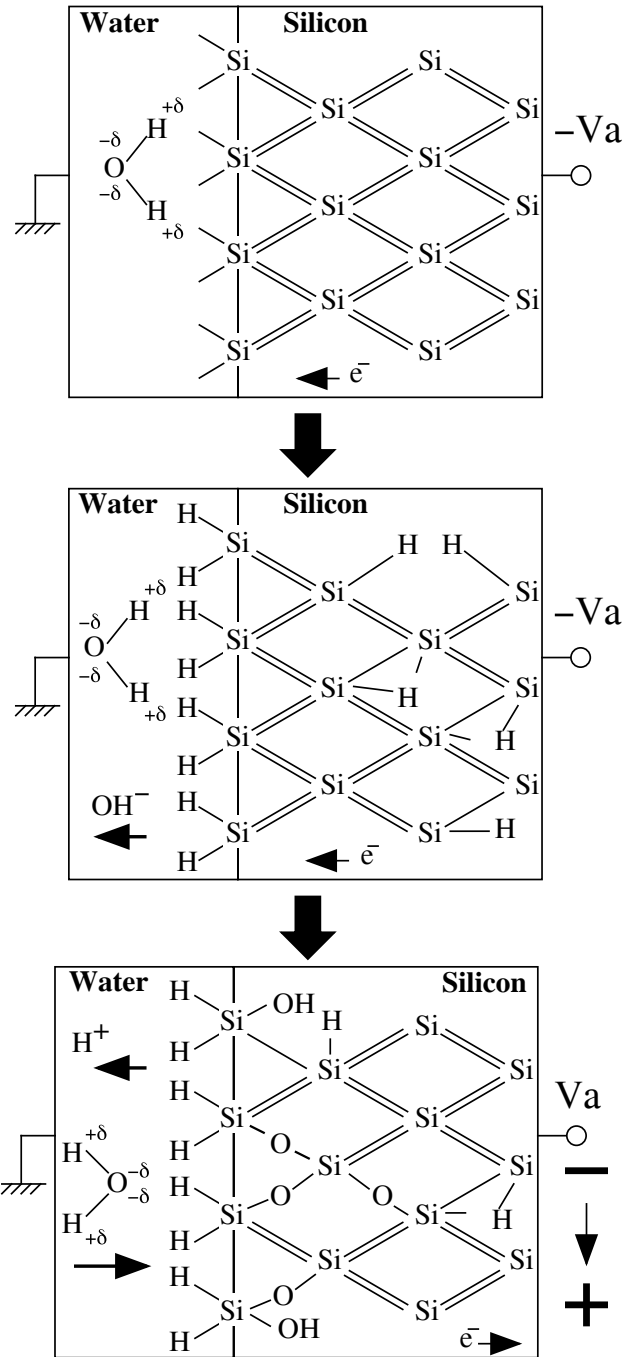


Fig. 14. Anodic oxidation model when the applied voltage changes from negative to positive.

charges near the water–Si interface are holes and are sharply distributed at the silicon surface. Therefore, OH and H react easily with silicon covalent bonds and dangling bonds, and form SiOH and SiH, respectively. In the case of an n-type silicon substrate, positive charges near the water–Si interface are ionized donors and holes that are minority carriers in an n-type substrate. There is a small number of holes compared with the case of the p-type substrate. Thus, the number of H and OH reacting with holes is smaller than for the p-type substrate.

5. Conclusions

We experimented with anodic oxidation in pure water at

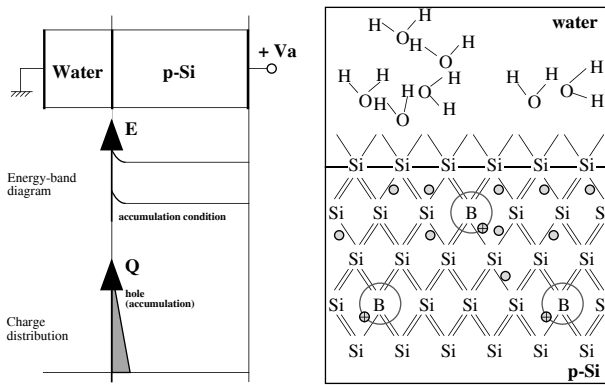


Fig. 15. Energy band diagram and charge distribution of n-Si surface.

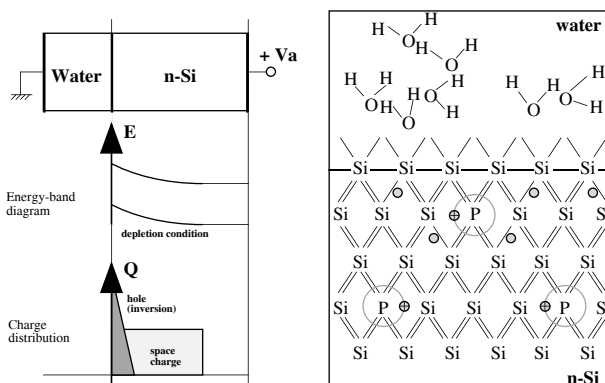


Fig. 16. Energy band diagram and charge distribution of p-Si surface.

room temperature as a possible low-temperature process and also discussed the growth mechanism using a model of molecular dipoles of water. We found that alternately changing the polarity of the applied voltage operates effectively to cause anodic oxidation. We also found that the composition of the oxide was stoichiometric SiO_2 , the oxide thickness increased with charges flowing during oxidation and the growth rate on p-type silicon was higher than on n-type silicon. The surface roughness was larger on n-type silicon than on p-type silicon. When the applied voltage polarity was changed alternately, surface roughness became small and the growth rate became twice that in the case of single polarity.

We also examined the possibility of improving the electrical characteristic of SiO_2 films by high-temperature annealing. The etching rate of the oxide film became small, and it was effective in decreasing the density of Si/ SiO_2 interface states and positive charge density in the oxide.

Our intention in performing this study is to apply the anodic oxide for the following purposes.

1. Low-temperature VLSI processes.
2. Bonded and Etched SOI.
3. Oxide film for micro-machining.

It is difficult to apply the anodic film to the LSI insulating film process directly. However, it will be possible to improve the quality by controlling the resistivity of pure water, substrate temperature and voltage stability. If the anodic oxide can be applied to an oxidized substrate to fabricate a BE-SOI wafer, an inexpensive SOI substrate can be obtained. We consider that the most realistic application at this stage is the use of the anodic oxide for micro-machining.

We attempted to apply the anodic oxidation to aid the suppression of global warming and environmental pollution, and made a tiny step toward the application of the electrical effect to the device fabrication process. We hope this study will contribute to positive changes in the use of energy.

Acknowledgement

We would like to thank Professor P. M. Lenahan of Pennsylvania State University for useful suggestions. We also wish to thank M. Saitou for experimental support and help with the figures. This work was supported partly by Fund of Research Project of College of Science and Technology, Nihon University.

- 1) Y. Numasawa, K. Yamasaki and K. Hamano: Jpn. J. Appl. Phys. **22** (1983) 792.
- 2) X. Wang, T. P. Ma, G. Cui, T. Tamagawa, J. W. Goltz, S. Karechi, B. H. Halpern and J. J. Schmitt: Jpn. J. Appl. Phys. **34** (1995) 955.
- 3) P. J. Jorgensen: J. Chem. Phys. **37** (1962) 874.
- 4) E. F. Duffek, C. Myroie and E. A. Bejamini: J. Electrochem. Soc. **111** (1964) 1042.
- 5) J. Kraitchiman and J. Oroshnik: J. Electrochem. Soc. **114** (1967) 405.
- 6) A. G. Revesz: J. Electrochem. Soc. **114** (1967) 629.
- 7) L. A. Dubrovskii, V. G. Mel'nik and L. L. Odyets: Russ. J. Phys. Chem. **36** (1962) 1183.
- 8) J. P. Hogan, A. M. Stoneham and M. Jaros: Philos. Mag. B **55** (1987) 225.

Preparations and Evaluations of C₆₀ Thin Films for Organic Field-Effect Transistors

Nobuyuki IWATA, Akane KINJO, Hiroki OKUYAMA and Hiroshi YAMAMOTO

Department of Electronics and Computer Science, College of Science and Technology, Nihon University,
7-24-1 Narashinodai Funabashi-shi, Chiba 274-8501, Japan

(Received June 25, 2004; accepted August 23, 2004; published January 24, 2005)

Fullerene C₆₀ thin films were grown on a mica top-gate-type substrate and on a CaF₂ // Si(111) bottom-gate-type substrate with the aim of fabricating high-performance organic field-effect transistors (FETs). It is expected that single-crystal C₆₀ thin films with a large grain have a high mobility as n-type materials because of the lack of a potential barrier at the grain boundaries for conducting electrons. On both substrates, oriented C₆₀ films were obtained. In particular, on the mica substrate, the highly oriented films had grains larger than 1 × 1 μm and a two-dimensionally flat surface with 60 and 120 deg facets. The step height was 0.8 nm, consistent with that of an *hcp* bulk structure. The highly oriented films were grown at the substrate temperature at which the C₆₀ molecules at the tips of spiral grains re-evaporated. The obtained single-crystal C₆₀ thin films with large grains are promising for high-performance organic FETs. [DOI: 10.1143/JJAP.44.617]

KEYWORDS: C₆₀, organic, mica, calcium fluoride (CaF₂), Si(111), thin film, FET, epitaxial growth, molecular beam epitaxy (MBE), atomic force microscopy (AFM)

1. Introduction

Recently, organic field-effect transistor (FET) devices have become attractive from the viewpoints of low cost, mechanical flexibility, low-temperature processing and so on. The performance of organic FETs should be comparable to that of amorphous silicon. Among organic semiconductors, pentacene has been well known as a p-type material because of its high mobility of 1.5 cm²/Vs, while n-type materials with high mobility are extremely desired for organic complementary circuits.¹⁾ Fullerene C₆₀ is expected as an n-type organic material. A practical *in-situ* measurement has demonstrated a high mobility of 0.5 cm²/Vs in a C₆₀ thin film.²⁾ In another study, alumina-passivated C₆₀ thin film with a mobility of 0.1 cm²/Vs prevents the degradation of FET performance.³⁾ However, there have been no reports focusing on how the crystallinity of the film and grain size affect FET performance for n-type organic semiconductors.⁴⁾ Therefore we tried to grow C₆₀ single-crystal thin films with a large grain in order to achieve a high FET performance. In such films, carrier transport is not suppressed because of few scatterings of carriers at grain boundaries.

In this study we discuss the single-crystal growth of C₆₀ thin films for two types of FET: top-gate type and bottom-gate type. Natural mica and CaF₂ // Si(111) were used as top-gate- and bottom-gate-type substrates, respectively. Calcium fluoride worked as a gate insulator and buffer layer for the growth of single-crystal C₆₀ thin films.

2. Experimental

Films were prepared using an ultra-high-vacuum molecular beam epitaxy (UHV-MBE) system with a background pressure of less than 1 × 10⁻⁸ Torr. The chamber for film growth and the prechamber for sample exchange were evacuated using a 2000 L/s diffusion pump and a 220 L/s turbomolecular pump, respectively. The substrate temperature, T_S, was measured using an optical pyrometer through the viewport of a ZnSe window. The powders of C₆₀ with 99.9% purity and of CaF₂ with 99.99% purity were evaporated from a pyrolytic boron nitride (PBN) crucible in effusion cells. Cell temperature for C₆₀ deposition was increased during growth in order to maintain a constant C₆₀

flux rate using a thickness monitor, while for CaF₂, it was kept constant at 1150°C, the flux of which was 1.9 × 10⁻⁴ Torr derived from the temperature dependence of steam pressure.

Cleaved natural mica substrates were set on the sample holder, where copper foils with 0.01 mm thickness were inserted between the holder and substrate for a better thermal contact and temperature uniformity. Prior to deposition the substrate was prebaked at 400°C for 60 min in vacuum. A growth rate of 3.0 nm/min was obtained for a film deposited on a glass substrate at room temperature. The pressure during C₆₀ film deposition was approximately 2.0 × 10⁻⁸ Torr.

The p-type Si (111) substrate for CaF₂ growth, the resistivity of which was less than 0.02 Ωcm, was cleaned ultrasonically for 60 s in Semicoclean23 solution (Furuuchi Chem. Co.) to remove organic impurities, etched by acid solution (HF:HCl:H₂O = 1:4:7) for 60 s and then rinsed with pure water. Those processes were carried out three times. Immediately the substrate settled on the sample holder with the insertion of 0.01-mm-thick Pt/Au foils and was loaded in the chamber. CaF₂ film is deposited at 250°C for 10 min and at 660°C for 60 min, at which the pressures were approximately 1 × 10⁻⁸ Torr and 8 × 10⁻⁸ Torr, respectively.

Surface morphology is observed by atomic force microscopy (AFM) (Seiko Instruments Inc. SII: SPI3800). The crystalline structures of the films are studied by X-ray diffraction analysis (XRD) (Rigaku: RAD-C).

3. Results and Discussion

3.1 C₆₀ films growth on mica substrate⁵⁾

Figure 1 shows a typical 2θ-θ XRD pattern of the C₆₀ thin film grown at 186°C on the mica substrate. From the consideration of each peak intensity, the XRD pattern of the film was assigned as that of an *hcp* structure rather than an *fcc* one. Other reflection peaks were found to originate from the substrate. The lattice spacing of C₆₀ (0002), fitted by a Nelson-Riley function, was 0.817 ± 0.001 nm, similar to that of *hcp* C₆₀ bulk, which is 0.818 nm.

Figure 2 shows the T_S dependence of the full width at half maximum (FWHM) of the (0002) Bragg reflection. The

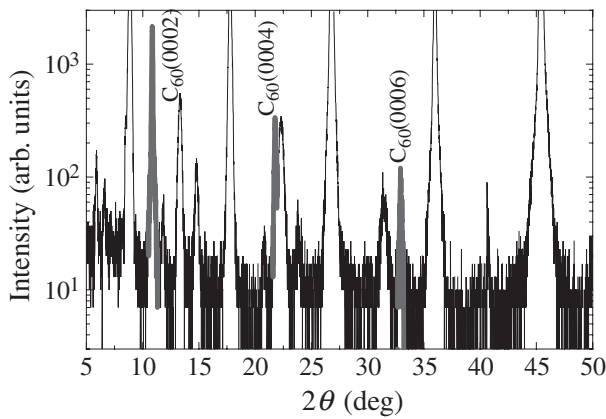


Fig. 1. XRD pattern of C_{60} film grown on mica substrate at 186°C . Bold peaks were indexed to C_{60} (0002), C_{60} (0004) and C_{60} (0006), respectively. The other peaks are attributed to the substrate.

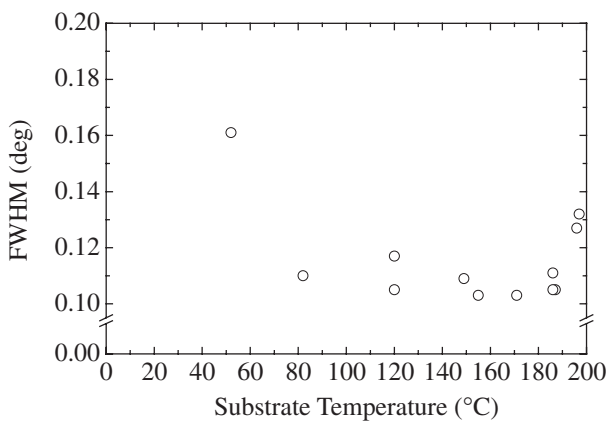


Fig. 2. Substrate temperature dependence of full width at half maximum (FWHM) of C_{60} (0002) Bragg reflection of film.

FWHM decreased up to 80°C and was constant at the T_S range from 80°C to 180°C . Above 180°C the FWHM rapidly increased. In general, the FWHM of the 2θ - θ Bragg peak depends on the fluctuation of lattice spacing and film thickness. In this case the FWHM should decrease with decreasing fluctuation and increasing temperature. The FWHM should increase with increasing temperature since film thickness decreased due to the re-evaporation of C_{60} molecules. These two factors resulted in the observed relationship of FWHM vs T_S .

Figure 3 shows the AFM images of a $2\ \mu\text{m}^2$ area of the C_{60} thin films grown at the temperature range from 40 to 120°C on mica substrates. The grains grown at 40°C with a grain size of $50\ \text{nm}$ were spread across the surface, as shown in Fig. 3(a). As substrate temperature increased the grain size also increased. Some of the grains grown at 80°C with a grain size of $150\ \text{nm}$ formed triangular structures, as shown in Fig. 3(b). For the grains grown at 100°C , the triangular structures can be clearly seen as shown in Fig. 3(c). Each grain was separated distinctly by grain boundaries. At 120°C the triangular grains began to coalesce, as shown in Fig. 3(d).

AFM images obtained at higher temperatures are shown in Fig. 4. The images on the left-hand side are of an area $2\ \mu\text{m}^2$ and those on the right-hand side are of an area $5\ \mu\text{m}^2$. The

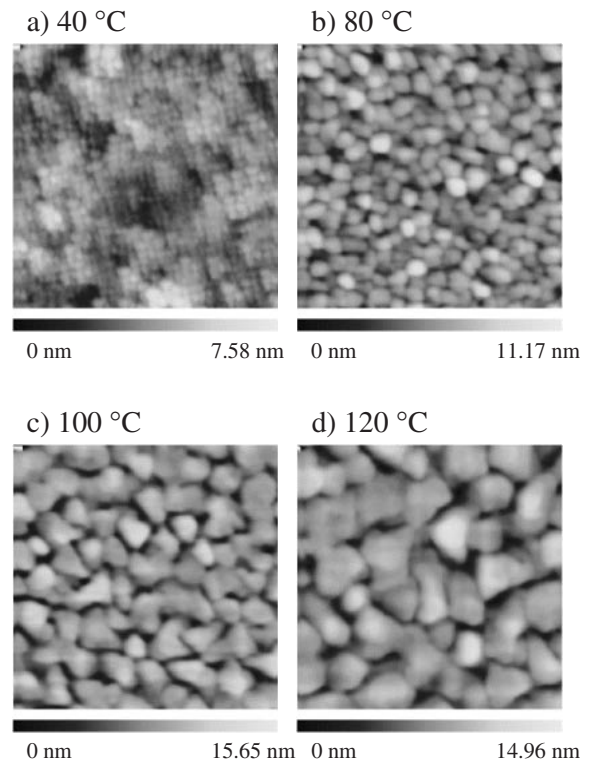


Fig. 3. AFM images of C_{60} films grown on mica substrate at substrate temperature range from 40 to 120°C .

coalesced grains had a spiral structure and were approximately $1 \times 1\ \mu\text{m}^2$ as shown in Figs. 4(a-1) and 4(a-2). Steps and terraces can be clearly observed. With increasing substrate temperature, terrace width increases. Separated grains are evident in Figs. 4(a-1) and 4(a-2) indicating the 3-dimensional (3D) growth mode. At 185°C , Figs. 4(b-1) and 4(b-2), the separated grains were not obvious, and spiral growth was obtained in some places on the 2-dimensionally flat surfaces of the C_{60} thin film, indicating 3D growth on the 2-dimensional (2D) surface. The terraces of the spiral grains sometimes had a discrete stack of terraces and/or screw dislocations, which could be from the incommensurate lattice match between the step height of the mica substrate and the radius of C_{60} .⁶⁾ At 197°C , Figs. 4(c-1) and 4(c-2), there was no spiral growth. Steps and terraces appeared with 60 and 120 deg facets, indicative of the 2D growth mode. The film thickness was less than $10\ \text{nm}$. Epitaxial growth with a single *hcp* structure took place in these films. Above this temperature, no film and no AFM images were obtained due to the re-evaporation of C_{60} .

The change in the growth mode probably occurred with increasing substrate temperature. However, at above 185°C , at which significant re-evaporation occurred, C_{60} molecules at the tip of the spirals should re-evaporate first. Eventually, the difference in the type of surface was caused not by the difference in growth mode but by the re-evaporation of C_{60} .

Figure 5 shows the AFM image at another point of the film shown in Figs. 4(c-1) and 4(c-2) with a line profile. The step height of $0.8\ \text{nm}$ was consistent with the lattice spacing of (0002) for the C_{60} *hcp* bulk structure.

The surface roughness R_a is shown as a function of T_S in Fig. 6. The R_a decreased linearly with increasing T_S up to

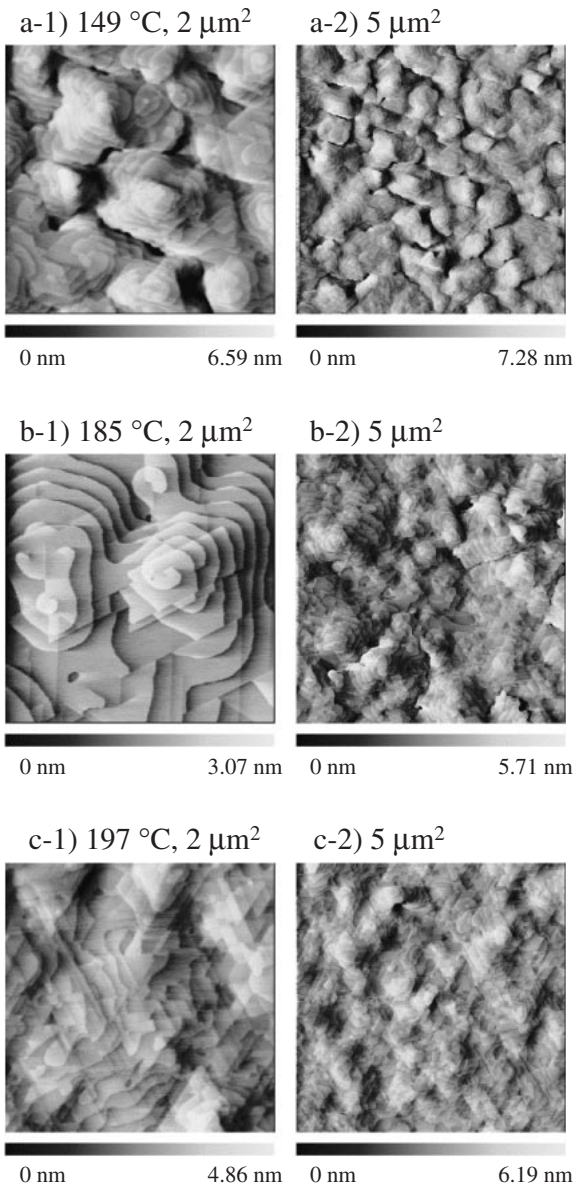


Fig. 4. AFM images of C_{60} films at higher substrate temperature range from 149 to 197°C. Left-hand side shows images of $2\mu m^2$ area and right-hand side shows images of $5\mu m^2$ area.

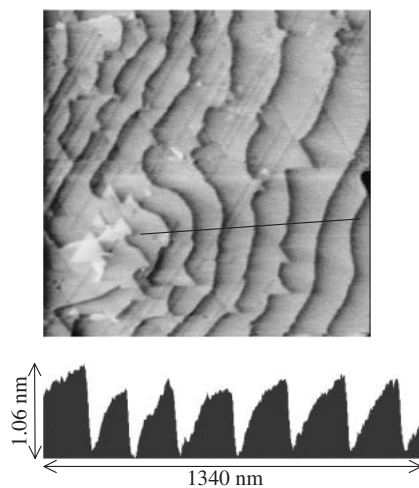


Fig. 5. AFM image and line profile are shown for film grown at 197°C. The height of the steps was 0.8 nm corresponding to the lattice spacing of C_{60} (0002).

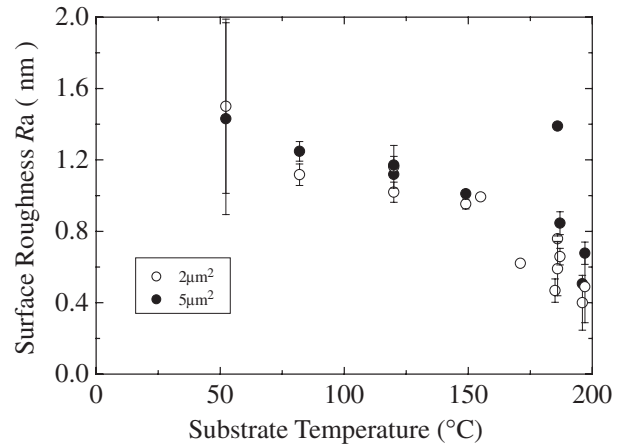


Fig. 6. Substrate temperature dependence of surface roughness R_a of C_{60} films prepared on mica substrates.

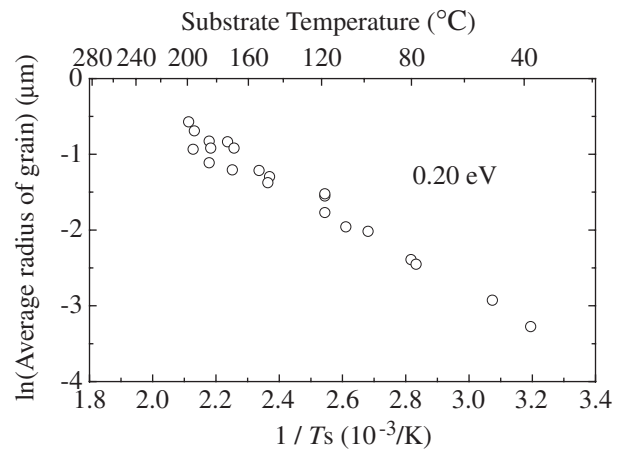


Fig. 7. Arrhenius plot for average radius of grains observed in films deposited on mica substrates.

150°C, and then rapidly decreased to a minimum. The rapid decrease was consistent with the difference in surface morphology due to marked re-evaporation of C_{60} molecules present at the tip of the spiral grain.

Using all the AFM images of the films prepared at various T_s 's, the Arrhenius plots of the average radius of the grains are drawn in Fig. 7 assuming that all the grains were spherical. The obtained data were fitted to a straight line for the wide range of T_s , though dispersion was slightly observed in the region of higher T_s . It was concluded that the growth mechanism can be explained by the simple model in which the C_{60} molecules migrate while thermally overcoming the activation energy of approximately 0.20 eV.

3.2 C_{60}/CaF_2 film growth on Si (111) substrate

The surface morphologies of CaF_2 and C_{60}/CaF_2 are shown in Fig. 8. Equilateral triangular grains with two-dimensionally flat terraces were observed with a side length of 100–800 nm and a height of 20–80 nm. The azimuth of the apex of triangular grains was along one direction, indicating epitaxial growth.

Generally, with increasing substrate temperature, decreasing flux and/or terrace width, the growth mode is transformed from pure terrace nucleation through a mixed step

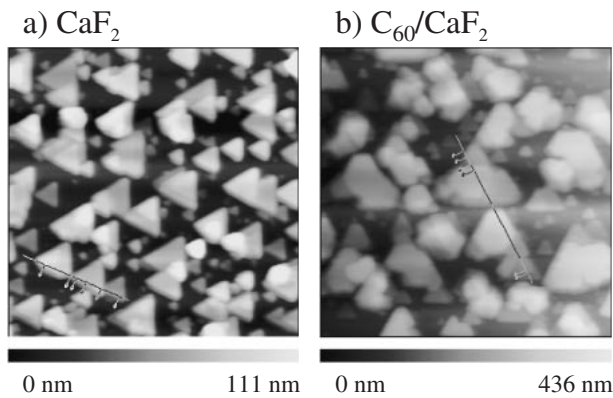


Fig. 8. AFM images of (a) CaF_2 film and (b) $\text{C}_{60}/\text{CaF}_2$ on Si(111) with size of $5\ \mu\text{m}^2$.

and terrace nucleation, to pure step nucleation and step flow.⁷⁾ Pure terrace nucleation is observed at approximately 600°C . The surface obtained was similar to that of the pure terrace nucleation at the substrate temperature of 660°C , which is the highest limit of our system. The flux rate of CaF_2 was rather low compared with that in the literature,⁷⁾ therefore smoother surfaces can be obtained on a substrate with narrower terraces.

As shown in Fig. 8(b), the C_{60} film was deposited on the $\text{CaF}_2 // \text{Si}(111)$ substrate at 190°C for 30 min. The surface morphology basically shows triangular grains which are obscure. The XRD profile shows the Bragg reflections of the *hcp* structure similar to that of the C_{60} film on the mica substrate.

4. Conclusion

Single-crystal C_{60} thin films were grown on a mica top-gate-type substrate and on a $\text{CaF}_2 // \text{Si}(111)$ bottom-gate-type substrate in order to achieve a high FET performance. It is expected that carrier transport is not suppressed because of the few scatterings of carriers at grain boundaries in the films

with large grains and then a high FET performance is achieved. On the mica substrate, a highly oriented *hcp* C_{60} film with a 2D flat surface grew just below the temperature above which C_{60} molecules totally re-evaporated. Two-dimensionally flat surfaces, which had a step and terrace structure with 60 and 120 deg facets, were achieved because of the re-evaporation of C_{60} molecules from the tip of the spiral grains. The height of the steps (0.8 nm) was consistent with that of *hcp* bulk. Grains larger than $1 \times 1\ \mu\text{m}^2$ were obtained. Under the same growth conditions as those for the mica substrate, an oriented *hcp* C_{60} film was obtained on the epitaxial $\text{CaF}_2 // \text{Si}(111)$ substrate, the surface of which showed equilateral triangular grains with a two-dimensionally flat terrace. The side length of the grains was 100–800 nm and the height of the grains was 20–80 nm. On both substrates, oriented C_{60} films were obtained. In particular the films on the mica substrate were promising as high-performance organic FETs.

Acknowledgement

The authors are grateful for the financial support of the Grant-in-Aid from the Futaba Electronics Memorial Foundation.

- 1) Y. Lin, D. J. Gundluch, S. Nelson and T. N. Jackson: *IEEE Electron Device Lett.* **18** (1997) 606.
- 2) S. Kobayashi, T. Takenobu and S. Mori: *Appl. Phys. Lett.* **82** (2003) 4581.
- 3) K. Horiuchi, K. Nakada, S. Uchino, S. Hashii, A. Hashimoto, N. Aoki, Y. Ochiai and M. Shimizu: *Appl. Phys. Lett.* **81** (2002) 1911.
- 4) C. D. Dimitrakopoulos and P. R. L. Malenfant: *Adv. Mater.* **14** (2002) 99.
- 5) N. Iwata, K. Mukaimoto, H. Imai and H. Yamamoto: *Surf. Coat. Tech.* **169–170** (2003) 646.
- 6) J. Fujita, S. Kuroshima, T. Satoh, J. S. Tsai, T. W. Ebbesen and K. Tanigaki: *Appl. Phys. Lett.* **63** (1993) 1008.
- 7) M. A. Olmstead: *Heteroepitaxy of Disparate Materials: From Chemisorption to Epitaxy in $\text{CaF}_2/\text{Si}(111)$* , eds. W. K. Liu and M. B. Santos (World Scientific Publishing Co., Pte., Ltd., Singapore, 1999), Chap. 5, p. 211.

Preparation of Nano-Structured C₆₀ Thin Films

Akane KINJO, Hiroki OKUYAMA, Nobuyuki IWATA and Hiroshi YAMAMOTO

College of Science and Technology, Nihon University, 7-24-1 Narashinodai, Funabashi-shi, Chiba 274-8501, Japan

(Received June 25, 2004; accepted October 26, 2004; published January 24, 2005)

Sapphire (0001) substrates were annealed at 1000°C for 12 h in air to obtain flat surfaces with a step-terrace structure. Au films were deposited on the substrates using the molecular beam epitaxy (MBE) method, at various substrate temperatures. The surface morphology of the films was observed by means of atomic force microscopy (AFM). A quasi one-dimensional alignment of Au particles was partially prepared along the steps at the substrate temperature of 620°C. On the other hand, an atomically flat Au thin film was obtained at the low substrate temperature of 130°C. A C₆₀ monolayer was obtained by re-evaporating the C₆₀ molecules deposited on the Au films, which was confirmed by X-ray photoelectron spectroscopy (XPS). [DOI: 10.1143/JJAP.44.736]

KEYWORDS: C₆₀ monolayer, nanostructure, step, terrace, diffusion barrier, atomic force microscopy (AFM)

1. Introduction

Recently, the fabrication of electronic devices has reached the nanoscale level with the continued increase in the density of integration. Therefore, the fabrication processes of devices are becoming increasingly complicated and costly. The aim of this study is to fabricate a nanoscale structure with functional molecules, in particular, a monolayer of C₆₀ molecules was aligned one- and/or two-dimensionally by a re-evaporation method. In this method, an important aspect is that the binding between C₆₀ and metals is stronger than that among the C₆₀ molecules. After the growth of C₆₀/Au and annealing, only those C₆₀ molecules directly adsorbed onto metals remained, whereas the molecules bound with a weak Van der Waals interaction were re-evaporated.

Then the alignment of metals is a particularly important process for obtaining nano-structured C₆₀ films. We have taken note of the surface structure of oxide single crystal substrates. A simple process has been reported for obtaining atomically flat surfaces with a step-terrace structure.^{1,2)} On such substrates, Au films were deposited by molecular beam epitaxy (MBE) while changing the substrate temperature. The surface morphology of the obtained films was observed and discussed with respect to the synthesis of nano-structured C₆₀ monolayers.

2. Experimental Procedure

Figure 1 shows the process proposed for the fabrication of C₆₀ low-dimensional structures, particularly the one-dimensional (1D) structure. (a) The substrates with step-terrace structures are prepared. (b) 1D Au alignments are formed along the steps of the substrates. It is expected that the steps function as a potential barrier for the migration of Au atoms and Au particles aligned along the steps. Therefore, a high substrate temperature and/or a low Au flux rate are a desirable condition. For the two-dimensional (2D) alignment of Au particles, a low substrate temperature is possibly an appropriate condition. (c) C₆₀ molecules are deposited on the substrates. (d) Annealing is carried out *in situ* to re-evaporate only those C₆₀ molecules bound with weak Van der Waals interactions.³⁾

Films were grown using an MBE system which was evacuated by a diffusion pump and a turbomolecular pump. The background pressure was approximately 1×10^{-8} Torr.

After the Al₂O₃ substrates are cleaned ultrasonically in

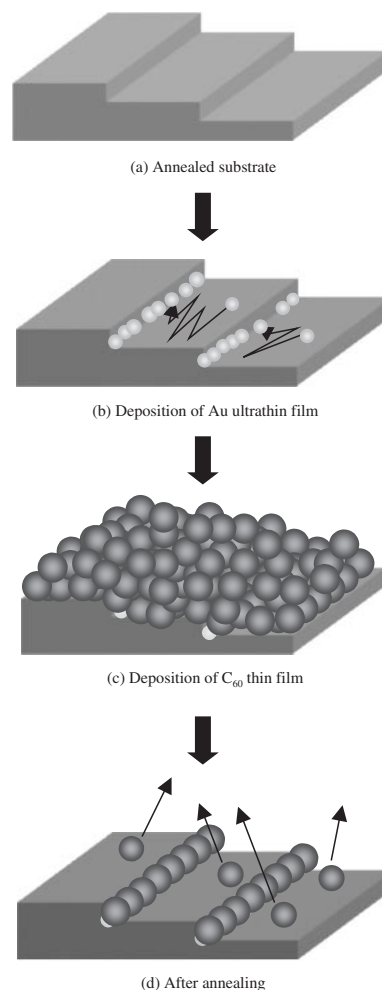


Fig. 1. Schematic images of proposed process for the fabrication of C₆₀ low-dimensional structures on Au layers. (a) Step-terrace structure of single crystal surface, (b) one-dimensional alignment of Au, (c) as-grown C₆₀ film and (d) one-dimensional alignment of C₆₀.

acetone, they are annealed at 1000°C for 12 h in air. The annealed substrates are pre-baked at 400°C for 30 min in vacuum, prior to the deposition. The growth temperatures of the substrates are measured using an optical pyrometer. Au with 99.99% purity and C₆₀ powder with 99.95% purity are evaporated from pyrolytic boron nitride (PBN) crucibles in Knudsen cells. Table I shows the details of conditions for

Table I. Conditions of film growth.

	K-Cell temperature (°C)	Substrates temperature (°C)	Deposition time (min)	Annealing after deposition
Au	1200–1300	130–630	1.5–40	130–630°C 30 min
C ₆₀	~350	190	5–10	~350°C 30 min

film growth. Au deposition is usually completed after the appearance of additional spots and/or rings of Au in the reflection high-energy electron diffraction (RHEED) pattern of the substrate. During the deposition, the temperature of the C₆₀ K-Cell is controlled in order to maintain a constant flux rate using a crystal thickness monitor.

The surfaces of the films were observed *in situ* by RHEED during deposition and annealing. After the air exposure of the samples, the surface morphology was measured by atomic force microscopy (AFM) (Seiko Instruments Inc. SII: SPI3800) and the chemical binding condition of C₆₀ was measured by X-ray photoelectron spectroscopy (XPS) (SHIMADZU Co.: ESCA-850, X-ray: MgK α). The XPS peaks were detected every 6 s during etching by Ar ions accelerated at 2 kV. The sample size was approximately 3 mm². Vertical differential charging was calibrated by the Au 4f_{5/2} peak.

Resistivity was measured by the four-point probe method. Comb-type Au electrodes were prepared on the substrate prior to the film deposition.

3. Results and Discussion

3.1 Surfaces of α -Al₂O₃ (0001) substrate

Figure 2 shows an AFM image of a sapphire (0001) substrate annealed at 1000°C for 12 h. The surface shows uniform parallel steps and atomically flat terraces with 0.21 nm step height and 80 nm terrace width. Uniform parallel steps are suitable for electrical conduction measurements of the Au particles one-dimensionally aligned along the steps.

3.2 One-dimensional structure

Figure 3 shows the AFM images of Au particles evaporated on the annealed substrates under the substrate temperature conditions (*T*_s) of (a) 350°C, (b) 500°C and (c) 620°C. The Au flux was fixed at 1.64 mTorr, which was derived from the temperature dependence of the equilibrium vapor pressure. The Au particles with diameters of approximately 10 nm were distributed without alignment at the *T*_s of (a) 350°C and (b) 500°C. At the *T*_s of (c) 620°C, particles had

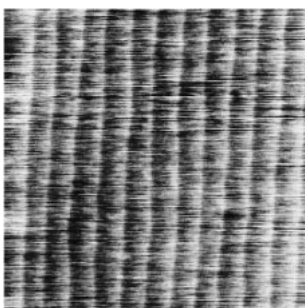
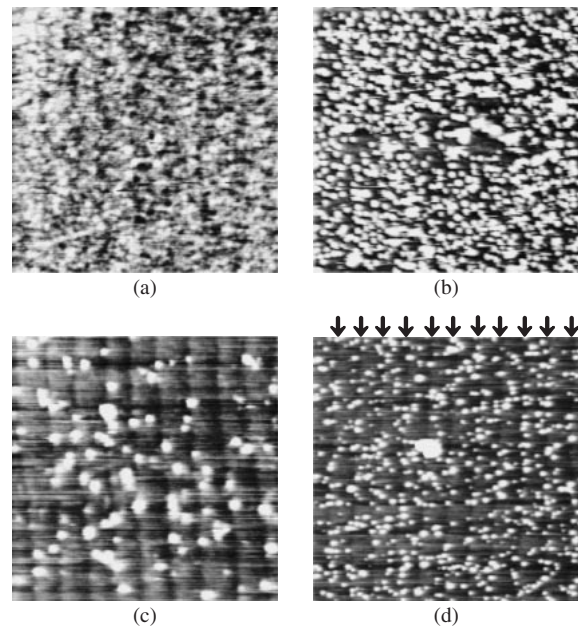
Fig. 2. AFM image (1000 nm²) of α -Al₂O₃ (0001) substrate.

Fig. 3. AFM images (1000 nm²) of Au particles deposited on α -Al₂O₃ (0001) substrate at different substrate temperatures of (a) 350°C, (b) 500°C, (c) and (d) 620°C. Au flux rates for (a)–(c) were 1.64 mTorr and that for (d) was 0.820 mTorr.

diameters of approximately 20 nm and were aligned partially along the lower and/or higher sides of the substrate steps. Figure 3(d) shows the AFM image of Au particles deposited at the *T*_s of 620°C under the Au flux of 0.820 mTorr. In this case, comparatively small Au particles with diameters of approximately 13 nm tended to align around the steps. From the comparison of the results in Figs. 3(c) with those in 3(d), it is confirmed that the diameter of the Au particles became smaller and the probability of the adherence of the Au particles at the steps became higher upon decreasing the flux rate.

By decreasing the flux rate and/or increasing the substrate temperature, the migration length of the deposited atoms increases. Therefore, the probability of the collision of atoms on the terraces was decreased, and then the deposited Au atoms reached the substrate steps and nucleated there. When atoms collide with other atoms on a terrace and grow beyond the critical radius of the nucleus, the collided particles do not reach the steps due to the higher potential barrier for migration, and thus they could form nucleation sites on the terrace. As shown in Fig. 3(d), the 1D nanostructure of Au particles appeared partially along the steps under the condition of *T*_s = 620°C and flux rate of 0.820 mTorr, under which condition the atoms can gain the migration energy required to reach the steps.

The Au particles become spherical as a general tendency because of the large difference in surface energy between Au and the substrate.⁴⁾ It is considered that comparatively small Au particles are more suitable for 1D alignment through connecting with each other along the steps than large particles are.

3.3 Two-dimensional structure

Figure 4 shows the RHEED patterns of (a) the annealed surface of sapphire (0001) substrates and (b) the Au thin film

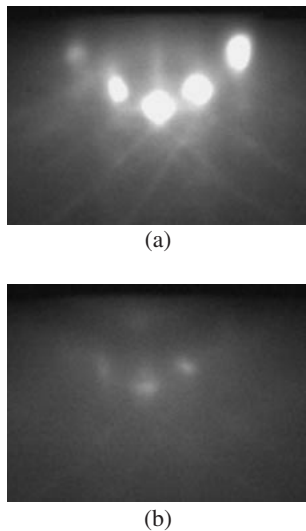


Fig. 4. RHEED patterns of (a) the annealed surface of α - Al_2O_3 (0001) and (b) deposited Au on Al_2O_3 substrate. Electron beam was incident from the $[1\bar{1}00]$ direction.

evaporated under the conditions of $T_s = 130^\circ\text{C}$ and the Au flux rate of 0.82 mTorr. The electron beam was incident from the $[1\bar{1}00]$ direction perpendicular to the step lines. After the deposition of Au, the characteristic pattern on the substrate disappeared and faint diffraction rings from Au were observed, indicating the growth of polycrystalline Au films.

Figure 5 shows an AFM image of the Au film. The image is similar to that of the substrate, which indicated an atomically flat Au thin film. This planar structured Au film was applied in the synthesis of a 2D structured C_{60} monolayer. The specimen was prepared by a process involving the deposition of C_{60} films on the 2D Au film and successive re-evaporation at 350°C .

Figure 6 shows an XPS spectrum of a C_{60} thin film after 6 s etching. This specimen was prepared on a Au thin film by the re-evaporation method. It is known that a monolayer of C_{60} on Au has a metallic property because of the charge transfer from Au to C_{60} and the XPS C1s peak with the tail extended to the higher binding energy side.^{5,6)} The observed asymmetric peak of the C_{60} film was consistent with the

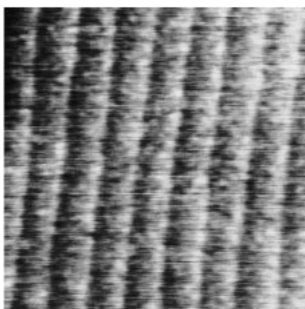


Fig. 5. AFM images (1000 nm^2) of deposited Au on Al_2O_3 at the substrate temperature of 130°C and flux rate of 0.820 mTorr.

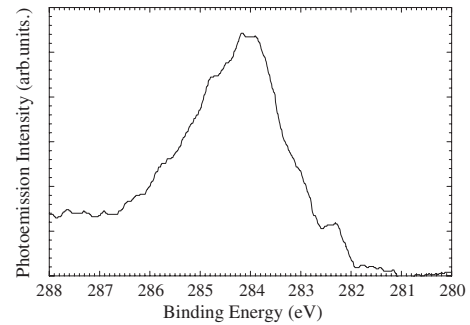


Fig. 6. XPS spectra of C1s peak of $\text{C}_{60}/\text{Au}/\text{Al}_2\text{O}_3$ (0001).

result for the C_{60} monolayer. Thus, it is apparent that the re-evaporation method is useful for the preparation of C_{60} monolayer on Au films.

The resistivity of the Au thin film was too high, namely, above $1\text{ k}\Omega\text{-cm}$, to be measured using our measurement system. However, it is expected that the electric conductivity of C_{60} monolayer can be measured and investigated in C_{60} films deposited on such a highly resistive Au film.

4. Conclusion

The 1D alignment of Au particles could be achieved on annealed α - Al_2O_3 (0001) substrates by increasing the substrate temperature and decreasing the flux rate because the steps function well as a potential barrier for the migration of Au atoms. The nanostructured 1D alignment of Au particles appeared partially along the steps under the condition of $T_s = 620^\circ\text{C}$ and flux rate of 0.820 mTorr.

Atomically flat 2D Au thin films were deposited at $T_s = 130^\circ\text{C}$ and the Au flux rate of 0.82 mTorr. After the C_{60} deposition on the Au thin film// Al_2O_3 (0001), the re-evaporation of C_{60} was carried out by annealing at 350°C . It was confirmed on the basis of XPS analysis that C_{60} monolayers can be synthesized on Au thin films by the re-evaporation method.

Acknowledgement

This work was supported by the Ministry of Education, Culture, Sports, Science and Technology through Scientific Grants-In-Aid (No. 12650322 & 15360173). The authors are also grateful for the financial support of a Grant-in-Aid from the Futaba Foundation.

- 1) M. Yoshimoto, T. Maeda, T. Ohnishi and H. Koinuma: *Appl. Phys. Lett.* **67** (1995) 2615.
- 2) Y. Shiratsuchi, M. Yamamoto and Y. Kamada: *Jpn. J. Appl. Phys.* **41** (2002) 5719.
- 3) E. I. Altman and R. J. Colton: *Surf. Sci.* **279** (1992) 49.
- 4) T. Ikoma *et al.*: *Ouyoubuturidetabukku* (Data Book of Applied Physics) (Maruzen, Tokyo, 1994) p. 290 [in Japanese].
- 5) J. E. Rowe, P. Rudolf, L. H. Tjeng, R. A. Malic, G. Meigs and C. T. Chen: *J. Mod. Phys. B* **6** (1992) 3909.
- 6) M. S. Dresselhaus, G. Dresselhaus and P. C. Eklund: *Science of Fullerenes and Carbon Nanotubes* (Academic Press, San Diego, 1996) Chap. 17.